

Received 1995 May 16; Accepted 1995 June 27; Publication date 1995, Dec. 20, v. 455,  
p 623, Astrophysical Journal

Following erratum submitted 29th January:

While reading the description of Figure 2, as well as the caption of the same Figure, it is to be noted that the solid, dashed, short dashed and dotted lines were drawn for  $\dot{m}_d = 0.001, 0.01, 0.1$  and  $1.0$  respectively. The sequence in inadvertently reversed in the text.

# SPECTRAL PROPERTIES OF ACCRETION DISKS AROUND GALACTIC AND EXTRAGALACTIC BLACK HOLES

Sandip K. Chakrabarti<sup>1</sup>

Code 665, Goddard Space Flight Center, Greenbelt, MD, 20771

and

Lev G. Titarchuk

George Mason University, 4400 University Drive, Fairfax, 22030

and

Code 668, Goddard Space Flight Center, Greenbelt, MD, 20771

August 8, 2018

## **Abstract**

We study the spectral properties of a very general class of accretion disks which can be decomposed into three distinct components apart from a shock at  $r = r_s$ : (1) An optically thick Keplerian disk on the equatorial plane ( $r > r_s$ ), (2) A sub-Keplerian optically thin halo above and below this Keplerian disk  $r > r_s$  and (3) A hot, optically slim,  $\tau \sim 1$  postshock region  $r < r_s \sim 5 - 10r_g$  where  $r_g$  is the Schwarzschild radius. The postshock region intercepts soft photons from the Keplerian component and reradiates them as hard X-rays and  $\gamma$  rays after Comptonization. We solve two-temperature equations in the postshock region with Coulomb energy exchange between protons and electrons, and incorporating radiative processes such as bremsstrahlung and Comptonization. We also present the exact prescription to compute the reflection of the hard X-rays from

the cool disk. We produce radiated spectra from both the disk components as functions of the accretion rates and compare them with the spectra of galactic and extragalactic black hole candidates. We find that the transition from hard state to soft state is smoothly initiated by a single parameter, namely, the mass accretion rate of the disk. In the soft state, when the postshock region is very optically thick and cooled down, bulk motion of the converging flow determines the spectral index to be about 1.5 in agreement with observations.

*Subject headings:* accretion, accretion disks – black hole physics – radiation mechanisms:nonthermal – shock waves –stars:neutron

<sup>1</sup> NRC Senior Research Associate; Address after October, 1995: Tata Institute of Fundamental Research, Homi Bhabha Road, Colaba, Bombay, 400005, INDIA

e-mails: chakraba@tifrvax.tifr.res.in; titarchuk@lheavx.gsfc.nasa.gov

# 1. INTRODUCTION

In the 1970s, the standard accretion disk models were constructed (Shakura & Sunyaev 1973; Novikov & Thorne 1973) to largely explain observations of binary systems. Matter supply from the companion is assumed to be through the Roche lobe and the angular momentum distribution is assumed to be Keplerian throughout the disk. Here, viscosity drives the inflow by removing angular momentum outward and keeping the entire disk Keplerian in the process. In the early 1980s, these disks became favorite candidates for the explanation of the “big blue bump” seen in the UV region of the active galaxies (Malkan 1982; Sun & Malkan 1989 and references therein) with some success.

With the advent of space based observations, the X-ray and  $\gamma$ -ray spectra of these objects show that there could be even bigger bumps in the X-ray regions of the spectra. Galactic black hole candidates such as GS1124-68, show two distinct spectral components, namely, soft and hard, which apparently vary quite independently (Tanaka 1989, hereafter TAN; Ebisawa et al., 1993, 1994 hereafter E93 and E94, respectively; Inoue 1992, hereafter I92). It was becoming clear that the standard accretion disks, which are in general cooler, cannot explain the production of X-rays and  $\gamma$ -rays. These models also cannot explain the almost zero time-lag correlated variabilities observed in, e.g., NGC4151, NGC5548 (Clavel et al. 1990; Peterson et al. 1991; Perola et al. 1986). Explanations of the hard components seen in the spectra of neutron star candidates and galactic and extragalactic black hole candidates required extra components, such as plasma clouds, hot coronae etc. which are not self-consistently constructed.

That the disks need not be of “standard” type was sensed by theoreticians since early 1980s (Liang & Thomson, 1980; Paczyński & Bisnovatyi-Kogan 1981; Muchotrzeb & Paczyński 1982; Paczyński & Wiita 1980; Abramowicz et al. 1988, Chakrabarti 1989, hereafter C89; Chakrabarti 1990ab, hereafter C90ab, Chakrabarti & Molteni 1995, hereafter CM95). Particularly, it was realized that the disks are not Keplerian everywhere,

especially at the inner boundary. (For a general discussion see, Chakrabarti 1995a, hereafter C95a). First global and fully self-consistent solution of viscous, transonic flows was obtained by C90ab who found that a Keplerian flow at the outer boundary can become sub-Keplerian at the inner edge (with or without shock waves). Or, contrarily, an initially sub-Keplerian flow can become almost Keplerian when viscosity is high enough. In a binary system, which includes a black hole or a neutron star, matter could be accreted from the winds of the companion at the same time as it is through the Roche lobe. In low mass X-ray binaries (LMXB), where companion winds may be scarce (except probably during outburst phase) the sub-Keplerian flow could come from the Keplerian disk itself as the advection becomes important closer to the black hole. In an active galaxy, the incoming matter is either a mixture of Keplerian and sub-Keplerian flows, or, entirely sub-Keplerian. This is because matter may be supplied from constantly colliding winds from a large number of stars  $\sim$  pc away and thus most of the angular momentum of the infalling matter may be lost. The above solutions, obtained in the context of isothermal flows, have been generalized since then for any heating and cooling (C95a; Chakrabarti 1995b, hereafter C95b) but no new topologies emerged.

After the matter starts with sub-Keplerian or Keplerian angular momentum  $l \leq l_{Kep}(r_{out})$ , its subsequent behavior depends strongly upon the accretion rate and the viscosity in the flow (C90ab; CM95, C95ab, Appendix). A unified description of what the flow might do (e.g., Fig. 4 of C89) suggests that, for a given entropy of the flow, if the accretion rate is small enough, the flow passes through the outer sonic point (just as in a Bondi flow) and remains supersonic before falling onto a black hole. If the accretion rate is high, matter would pass through the inner sonic point. In the intermediate case, matter is virtually stopped at a distance  $r_s$ , where  $l \simeq l_{Kep}(r_s)$  due to the centrifugal barrier, and a shock is formed. The postshock flow becomes highly subsonic momentarily, but picks up its velocity as it approaches the black hole eventually entering the horizon supersonically. The postshock region behaves similar to the thick accretion disks discussed in the literature (e.g., Paczyński & Wiita 1980) but is more self-

consistent as advection is explicitly added (C89, Molteni, Lanzafame, & Chakrabarti 1994, hereafter MLC94). In these solutions, the entropy of the flow passing through the inner sonic point is higher compared with the entropy of the flow passing through the outer sonic point. The combined effects of the shock and the viscosity generate the right amount of entropy to allow the flow to pass through the inner sonic point. The energy of the flow is either constant or very nearly so, because the energy and the entropy are advected with the flow toward the black hole. The advection is clearly important, since the radial velocity could be very high close to the black hole. When accretion rate is low enough, and shock conditions are not satisfied, a Keplerian disk would become sub-Keplerian close to the black hole at the same time becoming gas pressure dominated (Rees et al., 1982). Recently, importance of advection is stressed (‘newly discovered advection dominated flows’) by a simple self-similar analysis by Narayan & Yi (1994) who analyzes one of the branches of the solution topologies found by C90a,b.

The most general and complete global solution to-date of the viscous sub-Keplerian flow with advection (which becomes Keplerian at a larger distance), shows a very interesting behavior (C90a,b, CM95, C95b). When the viscosity is low [typically, when the viscosity parameter (Shakura & Sunyaev 1973) is less than a critical value,  $\alpha_v < \alpha_{vc}$ ], the shock can still form (depending on accretion rate, see C89) as in an inviscid flow, but as the viscosity is increased ( $\alpha_v > \alpha_{vc}$ ), the stable shock becomes weaker until it finally disappears. Numerical simulation provides insight into what actually happens (CM95). In the presence of viscosity, the rate of transport of angular momentum is faster in the postshock subsonic flow as compared with the preshock supersonic flow. As a result, angular momentum starts ‘piling up’ in the postshock flow and pushes the shock away to a larger distance. If one employs the Shakura-Sunyaev (1973) prescription, and the viscosity is small enough ( $\alpha_v \lesssim \alpha_{vc} \sim 0.01$  for isothermal disk, C90a), the transport rates could be matched and the shock settles down farther out. If the viscosity is higher, the transport rate is fast enough to push the shock to extinction and the flow becomes subsonic and Keplerian except close to the inner edge of the disk, where it passes through the inner sonic point. In the case of more general cooling and heating

laws,  $\alpha_{vc}$  could be anywhere between 0 to 1 depending upon the relative importance of cooling and heating (C95a,b). The predictions of shock locations and other properties from our vertically averaged model were found to agree with three dimensional simulations (MLC94). We, therefore, believe that these solutions are generally applicable even for quasi-spherical flow. This has also been noticed by recent self-similar study of Narayan & Yi (1994).

Numerical simulations (MLC94, see also Hawley et al. 1984, 1985; Ryu et al. 1995) also show that a strong wind forms in the postshock flow. Analytical works (C89) show that winds form when the specific energy of matter is positive and the specific entropy is high. The wind is found to become supersonic within a finite distance (MLC94). In the unified description (Fig. 4 of C89), the region of parameter space which produce winds (with and without shock waves) is discussed as well.

These, exact and global solutions (C90a,b, C95a,b) with higher viscosity, of the original model of transonic viscous disks of Paczyński and collaborators represent the most complete, Keplerian and quasi-Keplerian accretion disks in the literature. It has been suggested (Chakrabarti, 1993, hereafter C93, Chakrabarti, 1994, hereafter C94, C95a,b) that they go over to the so-called “thin”, “thick”, “slim” and “newly discovered advection dominated” and “cooling dominated” disks when appropriate approximations are made. Moreover, the solution of transonic viscous disk (C90a,b, CM95, C95a,b) also includes stationary shock waves for lower viscosity and appropriate accretion rate limit (C89). This ‘grand unification’ of disk models was possible, because the most general equations with all the solution branches including shocks are used (C93, C94, C95a,b) without making any further restrictive assumptions such as self-similarity (Narayan & Yi, 1994) or Keplerian distribution (Chen et al., 1995). Based on these solutions, one can construct the most general accretion disk close to a black hole. Assume for the moment that the flow is sub-Keplerian at the outer boundary and assume that the viscosity is higher on the equatorial plane and gradually drops with vertical height. The higher viscosity in the equatorial region re-distributes the sub-Keplerian angular

momentum and makes a standard, optically thick, Keplerian disk on the equatorial plane (CM95). However, the smaller viscosity at higher latitudes would produce an optically thin halo and this gas will pass through a shock close to the black hole, forming a very hot corona. In cases when an admixture of Keplerian and sub-Keplerian matter is supplied at the outer boundary (e.g., when both Roche lobe accretion and wind accretion are present) the segregation of this flow into two components is trivially achievable. In case where only Keplerian matter is supplied at the outer boundary, the disk can still be segregated in the same manner closer to the black hole depending on the viscosity variation and its vertical distribution which determines the region from which the flow starts deviating from Keplerian (C90a,b, Appendix). The solution with the shock (if available) is always chosen in place of the shock-free solution, as the former has a higher entropy (C89, MLC94).

Fig. 1 shows a cartoon diagram of the generalized accretion disk in presence of Keplerian and sub-Keplerian matter close to a black hole (also see, C94). An optically thick Keplerian disk is flanked by an optically thin, sub-Keplerian halo which passes through a standing shock close to the centrifugal barrier. The postshock region forms a hot ion pressure supported torus (e.g. Rees et al., 1982; MLC94) of moderate optical depth  $\tau \sim 1$  as the radial kinetic energy of the infall is thermalized:  $\rho v_r^2(r_s) \sim P \sim n_H k T_p$ . For matter with marginally bound angular momentum, the shock forms around  $r_s \sim 10r_g$  ( $r_g = 2GM/c^2$ , the radius of the black hole) in Schwarzschild geometry. The flow remains dissipative up to the marginally stable radius  $r_{ms} = 3r_g$ , beyond which the flow rapidly passes through the sonic point. For a flow around a Kerr black hole of angular momentum parameter  $a = 0.99$ , these length scales are roughly half as long. (Henceforth, we choose units of distance and velocity to be  $r_g$  and  $c$  respectively. We continue to use  $r$  to denote radial distances with this unit.) For higher angular momenta, shocks form farther away (C89). The postshock flow becomes geometrically thick, intercepting a few ( $\lesssim 5$ ) percent of the soft photons from the optically thick, Keplerian component of the preshock accretion disk. The postshock region with a Thomson optical depth of  $\tau_h \sim \int_{x_{ms}}^{x_s} 0.4 \rho dx$  ( $\sim 1 - 3$  for  $\dot{M} \sim \dot{M}_{Edd}$  rates) heats up



these soft photons through inverse Compton scattering (Sunyaev & Titarchuk 1980, hereafter ST80; Titarchuk 1994, hereafter T94; Titarchuk & Lyubarskij 1995; hereafter TL95 respectively.) and the photons are re-emitted which we claim to be responsible for the hard radiations from the accretion disks around galactic and extragalactic black holes. Some of these hard photons are intercepted by the Keplerian disk, a part of which is absorbed, thermalized, and reradiated by the disk as soft radiations, while the rest is reflected. We compute, completely self-consistently, the fraction of incoming hard radiation that each annulus absorbs or reflects away. Based upon our analysis, we do not find the component of hard radiation reflected from the disk to contribute significantly to the observed spectra. Secondly, we find the Keplerian disk component is not suitable for the site of the iron line emissions. Rather, we believe that the outflowing winds from the postshock flow (MLC94) or the evaporated preshock disk, could be the site of these lines at various stages of ionization (Chakrabarti et al., 1995, hereafter CTKE95). We shall touch upon this aspect of the problem in the final section. When the net accretion rate is high enough, cooler photons trapped in our postshock region are Comptonized by the ‘converging flow’ (e.g. Blandford & Payne, 1981) for  $r \leq r_{conv} \sim 3(\dot{M}_d + \dot{M}_h)/\dot{M}_{Edd}r_g$  where,  $\dot{M}_d$  and  $\dot{M}_h$  are the disk and halo rates respectively, and  $\dot{M}_{Edd}$  denotes the Eddington accretion rate. The resulting hard spectrum is very weak with a spectral slope of  $\alpha \sim 1.5$  ( $F_\nu \propto \nu^{-\alpha}$ ) and is characteristics of the spherical converging optically thick flow (Titarchuk, Mastichiadis & Kylafis 1995, hereafter TMK96).

The advantage of this model is that the soft and the hard radiations are formed self-consistently from the same accretion disk without invoking any ad hoc components such as the plasma cloud, hot corona, etc., whose origins have never been made clear. Secondly, our results are sensitive to only one parameter, namely, the disk accretion rate  $\dot{m}_d$ , although some observations suggest a variation of the halo accretion rate  $\dot{m}_h$  cannot be ruled out. In the next Section, we present the equations for the hydrodynamics and radiative processes which we use to describe our model. In §3, we present the results and physical interpretations of our solution. In §4, we present general comparisons with

observations. In §5, we make concluding remarks.

## 2. THE MODEL DESCRIPTION AND THE BASIC EQUATIONS

### 2.1 Description of the Model

As mentioned in the introduction, our model consists of two major disk components:

(1) The Standard Disk Component: A standard, optically thick disk could be produced either from the Keplerian or the sub-Keplerian matter at the outer boundary, if the viscosity and cooling are appropriate (C90a,b, CM95, C95a,b, Appendix). While constructing the equatorial Keplerian disk, we therefore incorporate the usual assumptions regarding the flux emitted from the disk. We assume that before the shock is formed at  $r=r_s$ , there is a thin, standard, Keplerian disk on the equatorial plane which, in the absence of the shock, would emit a flux of (e.g, Shapiro & Teukolsky 1984)

$$F_{SS} = 7.6 \times 10^{26} r^{-3} \mathcal{I} \left( \frac{M}{M_\odot} \right)^2 \frac{\dot{M}}{1.4 \times 10^{17}} \text{erg cm}^{-2} \text{s}^{-1}. \quad (1)$$

Here  $\mathcal{I} = 1 - (3/r)^{1/2}$ . In the presence of the shock at  $r_s$ , this component continues till  $r_s$ . The soft radiation luminosity  $L_S$  is then the integral of the above flux from  $r_s$  outwards plus the intercepted radiation coming from the postshock region:

$$L_S = L_{SS} + L_H f_{sd} (1 - \mathcal{A}_\nu), \quad (2)$$

where,  $\mathcal{A}_\nu$  is the albedo of the disk,  $L_H \sim L_{SS} f_{ds} E_{Comp}$  is the hard luminosity from the postshock region,  $f_{sd}$  is the fraction (determined by the geometry) of  $L_H$  that is intercepted by the disk, and  $E_{Comp}$  is the factor by which the soft photons incident on the postshock region (fraction  $f_{ds}$  of  $L_{SS}$ ) is enhanced due to Comptonization. The second term therefore represents the luminosity of the soft photons resulting from reprocessing of the hard radiation intercepted by the Keplerian disk.

(2) Sub-Keplerian Halo Component: We consider in detail the properties of the sub-Keplerian halo component and the effects of the halo on the emission properties of the Keplerian component. We assume the halo to be quasi-spherical and axisymmetric. For the purpose of obtaining the height of the shock, we assumed the flow to be in vertical equilibrium in the postshock region. The height of the shock enables us to compute the fraction  $f_{sd}$  of disk soft photons intercepted by the shock as well as the fraction  $f_{ds}$  of hard radiations from the shock intercepted by the disk. We assume the polytropic index to be  $\gamma=5/3$  in the halo. A  $\gamma=5/3$  spherical adiabatic flow cannot have a shock (C90b), but if the flow is thin, it can have two sonic points and therefore a standing shock. Even when a flow has only the inner sonic point, a shock can form if it is already supersonic at the source. An effective polytropic index is likely to be  $4/3 > \gamma > 5/3$ , but we do not expect any change of our general conclusions. Since we are interested in accreting solutions, the angular momentum in the halo component should be around the marginally bound and marginally stable values. In this low angular momentum regime, in the Schwarzschild geometry, the shock may be located around  $r_s = 10-30$  or so (C89). The inner edge of the postshock flow is extended till only the inner sonic point  $r_i$ , since for  $r < r_i$ , advection is so strong that matter may be considered radiatively inefficient. Since the inner sonic point is close to the marginally stable orbit  $r_{ms} = 3$  anyway, we integrate the equations only from  $r_s$  to  $r_{ms}$ . We also considered the solutions around a Kerr black hole, where  $r_s \sim 5$  and  $r_{ms} \sim 1.5$  will be employed. These are reasonable values for  $a \sim 0.99$ . The results are similar, though vary only in details. Flow within the inner sonic point constitutes the so-called convergent inflow provided the accretion rate is high enough which produces the characteristic weaker hard component as will be discussed later.

## 2.2 Hydrodynamics

We solve two temperature equations for the sub-Keplerian halo component and the postshock region. We ignore the vertical structure of the halo and use the vertically integrated equations. Comparison of analytical (C89) and numerical simulations

(MLC94) show that such assumptions are justified. The radial momentum equation is given by,

$$v_r \frac{dv_r}{dr} + \frac{1}{\rho} \frac{dP}{dr} - \frac{l^2}{r^3} + \phi(r) = 0, \quad (3a)$$

where  $P$  and  $\rho$  are vertically integrated pressure and density, respectively,  $l$  is the specific angular momentum and  $\phi(r) = -1/2(r-1)^{-1}$  denotes the Paczyński-Wiita (Paczynski & Wiita, 1980) potential which mimics the geometry around a black hole quite well. The variation of the azimuthal angular momentum in presence of viscosity is given by

$$v_r \frac{dl}{dr} - \frac{1}{hr\rho} \frac{d}{dr}(r^2 W_{r\phi}) = 0. \quad (3b)$$

We assume the viscosity in the halo to be small enough ( $\alpha_v < \alpha_{vc}$ ) so that the centrifugal barrier can form a shock in the halo (C90a,b, CM95, C95a,b). However, we assume the viscosity on the equatorial plane to be high enough so that the angular momentum there is Keplerian. This would produce a generic composite disk with optically thick (Keplerian disk), thin (sub-Keplerian halo) and slim ( $\tau \sim 1$ , postshock region) components. Whether all the three components will be present will depend on viscosity and cooling processes. Detailed classification of global solutions will be discussed elsewhere (C95b).

In the region,  $r < r_s$ , the Keplerian and sub-Keplerian components can behave identically for three reasons: (1) the angular momenta of the sub-Keplerian and Keplerian components are roughly the same at the centrifugal barrier, i.e., at  $r \lesssim r_s$ ; (2)  $v_r \approx 0$  in the immediately postshock region of the halo whereas  $dv_r/dr \approx 0$  in the disk component (velocity shoots up from a minimum, C89, C95b, Case A in Fig. 10 of Appendix A) — in either case the advection term  $v_r dv_r/dr$ , in the immediate vicinity of the shock is negligible and both the flows accrete downstream as a single component, and, most importantly, (3) since the postshock region is much hotter (more than 2 to 3 orders of magnitude, see, §3) than the Keplerian component, it evaporates the disk underneath and together they are expected to behave as a single component (Fig. 1) provided the mixing of the disk and halo are efficient. In the present paper we assume

that the turbulent mixing time is slower than the infall time scale. In a neutron star accretion the mixing is complete. This case will be discussed elsewhere.

The optically thin preshock halo does not radiate efficiently and therefore advects the energy and entropy along with the flow exactly as in our previous model of transonic disks (C89; C90a,b; C95b). In the postshock region, the disk will be hotter. If the flow is in hydrostatic equilibrium in the vertical direction, Mach numbers at the shock are related by (C89, C90b):

$$\frac{[M_+(3\gamma - 1) + \frac{2}{M_+}]^2}{2 + (\gamma - 1)M_+^2} = \frac{[M_-(3\gamma - 1) + \frac{2}{M_-}]^2}{2 + (\gamma - 1)M_-^2}. \quad (4a)$$

(The subscripts “-” and “+” denote the preshock and postshock quantities, respectively.) Assuming a strong shock, it is easy to show that the post shock Mach number is  $M_+ \sim 0.35$  which gives the postshock proton temperature as:

$$T_p \sim 1.56 \times 10^{12} r_s^{-1} K. \quad (4b)$$

However, if the flow were not assumed to be in vertical equilibrium, but remained thin, a different Mach number relation is to be used (C90b):

$$\frac{(M_+\gamma + \frac{1}{M_+})^2}{2 + (\gamma - 1)M_+^2} = \frac{(M_-\gamma + \frac{1}{M_-})^2}{2 + (\gamma - 1)M_-^2}. \quad (5a)$$

In this case, the postshock Mach number for a strong shock is  $M_+ = 0.45$ , and the proton temperature in the postshock region is,

$$T_p \sim 0.96 \times 10^{12} r_s^{-1} K \quad (5b)$$

For a spherical flow with  $\gamma \sim 5/3$ , shocks can form if the accreted sub-Keplerian matter is already supersonic (this is true for models in vertical equilibrium if  $\gamma \gtrsim 1.5$ , C95a) but for a thinner flow even with  $\gamma = 5/3$  there are two saddle type sonic points and shocks could form. Subsequent behavior of the protons and electrons will depend on the heating and cooling processes. As the matter accretes, it is compressed due to geometrical effects and becomes hotter. At the same time, the electrons lose energy due to bremsstrahlung and Comptonization of the soft photons from the disk. They also

gain energy from the protons due to the Coulomb interactions, and cool the protons in the process. The energy equation which the protons and electrons obey in the postshock region is:

$$\frac{\partial}{\partial r}(\epsilon + \frac{P}{\rho}) + (\Gamma - \Lambda) = 0, \quad (6)$$

where  $\epsilon$  is given by,

$$\epsilon = \frac{1}{2}v_r^2 + \frac{P}{\rho(\gamma - 1)} - \frac{1}{2(r - 1)} + \frac{l^2}{2r^2}, \quad (7)$$

and  $\Gamma$  and  $\Lambda$  are the heating and cooling terms respectively.

In the equation which governs the proton energy, we consider  $\gamma = 5/3$  and no heating. We consider the coolings to be due to inverse bremsstrahlung, and the transfer of energy to the electrons by Coulomb coupling. In the equation which governs the electron energy, we use heating due to transfer of energy from protons through Coulomb coupling and cooling due to bremsstrahlung and Comptonization. If the electron temperature  $T_e$  is high enough,  $kT_e > m_e c^2$  (where,  $m_e$  is the mass of an electron), we use  $\gamma = 4/3$ , otherwise we use  $\gamma = 5/3$ . Synchrotron losses could be trivially added to our equations. Since this requires a knowledge of unknown magnetic field contents, we ignore its effects for the time being. The temperature at the shock is not high enough to induce a significant pair production, so we ignore these effects. Within the convergent flow regime  $r < 2 - 3r_g$ , in optically thick flow, pair production will take place which may be responsible for the annihilation lines observed in soft state.

## 2.3 Radiative Processes

The bremsstrahlung and Coulomb cooling rates are taken from the standard texts (e.g., Lang 1980). Correct Comptonization rates have been computed very recently (T94; TL95) and we discuss them here for the sake of completeness. We provide new results on the computation of reflection of the hard radiation from the cooler disk.

### 2.3.1 Comptonization

Comptonization is the problem of energy exchange in the scattering of photons off the electrons. In the postshock plasma, as the accretion rate increases and the Thomson opacity,

$$\tau_T = \int_{r_i}^{r_s} \sigma_T n_e dr, \quad (8)$$

approaches unity, the escaping photons gain energy due to repeated scattering with the hot electrons. For a thermal non-relativistic electron distribution with a temperature  $T_e$ , the average energy exchange per scattering is given by ( $h\nu, kT_e \ll m_e c^2$ ),

$$\frac{\langle \Delta\nu \rangle}{\nu} = \frac{4kT_e - h\nu}{m_e c^2}. \quad (9)$$

When  $h\nu \ll kT_e$ , photons gain energy due to the Doppler effect and when  $h\nu \gg kT_e$ , photons lose energy because of the recoil effect. As the radiation passes through the medium, the probability of repeated scattering by the same photon decreases exponentially although the corresponding gain in energy is exponentially higher. A balance of these two factors yields a power law distribution of the energy density:

$$F_\nu \propto \nu^{-\alpha}. \quad (10)$$

In the limit of high energies ( $h\nu \gg kT_e$ ) the exponential hard tail is formed as a result of the recoil effect (the photons are unable to gain more energy than electrons actually have:  $h\nu \propto kT_e$ ).

It is shown in TL95 that the power laws are the exact solutions of the radiative transfer kinetic equations taking into account the Doppler effect only. The related spectral indices are derived for a wide range of the optical depths and electron temperatures of the plasma cloud from the following transcendental equation as follows:

$$\alpha = \frac{\beta}{\ln[1 + (\alpha + 3)\Theta / (1 + \Theta) + 4d_0^{1/\alpha}\Theta^2]}, \quad (11)$$

where

$$d_0(\alpha) = \frac{3[(\alpha + 3)\alpha + 4]\Gamma(2\alpha + 2)}{(\alpha + 3)(\alpha + 2)^2},$$

and  $\Theta = kT_e/m_e c^2$  which represents the appropriately weighted average of the electron temperature in the postshock region is computed from the model. Here,  $\beta$  is obtained

from the eigenvalue  $\zeta = \exp(-\beta)$  of the corresponding eigenfunction for the appropriate radiative transfer problem. If we approximate the postshock region as a slab, for optical depths  $\tau_0 > 0.1$ ,

$$\beta = \frac{\pi^2}{12(\tau_0 + 2/3)^2}(1 - e^{-1.35\tau_0}) + 0.45e^{-3.7\tau_0} \ln \frac{10}{3\tau_0}, \quad (12a)$$

and for very low optical depth  $\tau_0 < 0.1$ ,

$$\beta = \ln \left[ \frac{1}{\tau_0 \ln(1.53/\tau_0)} \right]. \quad (12b)$$

If on the other hand, the postshock region is approximated as a spherical bulge, then for optical depths ( $\tau_0 > 0.1$ ),

$$\beta = \frac{\pi^2}{3(\tau_0 + 2/3)^2}(1 - e^{-0.7\tau_0}) + e^{-1.4\tau_0} \ln \frac{4}{3\tau_0}, \quad (13a)$$

and for very low optical depth ( $\tau_0 < 0.11$ )

$$\beta = \ln \frac{4}{3\tau_0}. \quad (13b)$$

In Hua & Titarchuk (1995, hereafter HT95) the Comptonization spectra are given for the optically thin ( $\tau_0 < 1$ ) and thick ( $\tau_0 > 1$ ) regimes. There is a good approximate formula combining both regimes (HT95 Eq. [9]) which we use in our spectral calculations.

From the numerical simulation of the three dimensional flows (MLC94), it is evident that the postshock region behaves more like a thick accretion disk (Rees et al. 1982; Paczyński & Wiita 1980). Thus, it is neither a slab nor a sphere, but approximately a torus. Therefore, one expects the spectral index to be somewhat in between these two limits. However, as one goes inward, the optical depth rises and the contribution to the external hard radiation field diminishes. Therefore, either of these two assumptions should give sufficiently accurate results. The results we provide in the next section assumes the geometry of the hot region to be spherical. This assumption is made only to obtain an appropriately averaged electron temperature to compute the emergent hard spectra.



For our self-consistent calculation of the temperature distribution of the shock region we use the expression of the Comptonization enhancement factor  $E_{Comp}$  as a function of the spectral index  $\alpha$  and the effective low-frequency (temperature  $T_r$ ) dimensionless photon energy  $x_0 = 2.7kT_r/kT_e$

$$E_{Comp} = \begin{cases} q_{x_0}(\alpha)x_0^{\alpha-1}, & \text{if } \alpha < 1; \\ \frac{\alpha(\alpha+3)(1 - \frac{\alpha+4}{2\alpha+3}x_0^{\alpha-1})}{(\alpha+4)(\alpha-1)}, & \text{if } \alpha \geq 1. \end{cases} \quad (14)$$

where,

$$q_{x_0}(\alpha) = \frac{\alpha(\alpha+3)\Gamma(\alpha+4)\Gamma(\alpha)\Gamma(1-\alpha)}{\Gamma(2\alpha+4)}(1 - x_0^{1-\alpha}).$$

This formula, obtained by integration of the emergent spectrum over the photon energy covers asymptotic forms for both the regimes ( $\alpha < 1$  and  $\alpha \geq 1$ ) which are presented in ST80, Sunyaev & Titarchuk (1985, hereafter ST85).

### 2.3.2 Computation of the Reflected Component

Because a great deal of importance has been given in recent literature on the possibility of observation of the reflected component (e.g., Zdziarski et al., 1990; Done et al. 1992; Haardt et al., 1993), we address this issue here in detail. We find angle and energy dependent analytical solution (for  $E < m_e c^2$ ) which is applicable when the reflector (disk) is cold ( $\lesssim 10^5 \text{K}$ ). For a hotter disk, the reflection is more efficient because the photoelectric absorption process is considerably weak (Kallman & Krolik, 1986). We have incorporated this effect by neglecting the photoelectric absorption term (eq. 19-21 below) for  $T \gtrsim 10^5 \text{K}$ . Our computation of the equivalent width in terms of a cold disk reflection only gives an upper limit, since it is smaller for any hotter disk.

In computation of the reflected hard component, we note that the reflection spectrum from the disk is a result of scattering of the hard radiations from the shock by the relatively cold matter of the disk. They suffer photoelectric absorption at energies less than 10 keV with emission of the strong  $K_\alpha$  line and down-scattering (recoil effect) at energies higher than 50 keV. Thus, the reflection spectrum has a maximum at an energy around 15 – 20 keV. In order to estimate the reflected flux one requires a knowledge of

the fraction  $f_{sd}$  of the shock hard radiation intercepted by the disk and the reflection properties of the disk. In the very nonrelativistic energy range  $\leq 30\text{keV}$ , photons scatter off electrons almost coherently and consequently the results of the classical reflection problem (see e.g., Chandrasekhar 1960) are applicable, i.e., the intensity reflected from the disk at angle  $\theta = \cos^{-1} \mu$  (with respect to the disk normal) when the incoming hard flux  $\pi F_H$  falls onto the disk at the angle  $\theta_0 = \cos^{-1} \mu_0$  is as follows

$$I(\mu, \mu_0) = \frac{\lambda_\nu F_H f_{sd}}{4} \frac{H(\mu, \lambda_\nu) H(\mu_0, \lambda_\nu)}{\mu + \mu_0}. \quad (15)$$

Here,

$$\lambda_\nu = \{[1 + [Y + Y_0 \cdot \Theta(E - 7.11\text{keV})](7.8 \text{ keV}/E)^3]\}^{-1}, \quad (16)$$

is the photon scattering probability in the presence of photoelectric absorption,  $H(\mu, \lambda_\nu)$  is the well known H-function which changes within a range of 1–3 or even less depending on the photon scattering probability (see e.g., Chandrasekhar, 1960),  $Y$  and  $Y_0$  are the abundances of elements (in units of the cosmic abundance) with a charge  $Z < 26$  and the iron abundance, respectively.  $\Theta(x)$  is the Theta-function (0 for  $x < 0$  and 1 for  $x > 0$ ). At the hard tail, the intensity can be presented as a product of the three factors, namely  $I(\mu, \mu_0) = F_H f_{sd} \mathcal{A}_\nu(\mu, \mu_0)$ , where  $\mathcal{A}_\nu(\mu, \mu_0)$  is the albedo of the cooler disk.

### *Computation of Albedo*

In the computation of the albedo  $\mathcal{A}_\nu(r, \mu, \mu_0)$  of the disk, same two processes are to be taken into account: the recoil effect and the photoelectric absorption. In the presence of the recoil effect alone, the incident radiation of frequency  $\nu$  will be completely absorbed, if (ST80, Titarchuk 1987, hereafter T87)

$$\frac{\Delta\nu}{\nu} \sim \frac{h\nu}{m_e c^2} \tau_0^2 = z\tau_0^2 \sim 1 \quad (17)$$

i.e.,

$$\tau_0 \sim \frac{1}{z^{1/2}}. \quad (18)$$

The albedo  $\mathcal{A}_\nu$  would be  $1 - 1/\tau_0 = 1 - \sqrt{z}$ . In the presence of photoelectric absorption, similarly  $\tau_0^2(1 - \lambda_\nu) \sim 1$  and  $\mathcal{A}_\nu = 1 - 1/\tau_0 = 1 - \sqrt{\delta_\nu}$ , where,

$$\delta_\nu = 1 - \lambda_\nu = \frac{[Y + Y_0 \cdot \Theta(E - 7.11\text{keV})](z_*/z)^3}{1 + [Y + Y_0 \cdot \Theta(E - 7.11\text{keV})](z_*/z)^3}$$

( $z_* = 7.8 \text{ keV}/511\text{keV}$ ) is the probability of the photoelectric absorption (see, Eq.16).

In the presence of both recoil and photoelectric absorption, and taking into account the angular dependence of the incoming and outgoing radiations, we (see T87) obtain a more accurate expression for albedo as a function of the frequency of the incoming radiation and the angle of incidence  $\theta$  as,

$$\mathcal{A}_\nu = 1 - \phi(\mu_0)\Delta, \quad (19)$$

where

$$\phi(\mu_0) = \frac{1 + \sqrt{3}\mu_0}{1 + \sqrt{3(1 - \lambda_\nu)}\mu_0} \left[ 1 - \frac{\lambda_\nu\mu_0}{4} (1 + \lambda_\nu^2)(\ln \mu_0 + 1.33 - 1.458\mu_0^{0.62}) \right], \quad (20)$$

$$\Delta = (1 - \lambda_\nu)^{1/2} = \left[ \sqrt{z} \exp\left(\frac{\delta_\nu}{z}\right) \text{erfc}\left(\frac{\delta_\nu^{1/2}}{\sqrt{z}}\right) + \delta_\nu^{1/2} \right], \quad (21)$$

and  $\mu = \cos \psi$  where  $\psi$  is the angle which the incident radiation subtends with the local normal to the disk. The second term is negligible for  $T \gtrsim 10^5 \text{K}$ .

### 2.3.2.2 The analytical solution of the reflection component

The problem of the reflection from the cold material is related to the radiative transfer kinetic equation which takes into account the photoelectric absorption and the recoil effect (see e.g. Basko, Sunyaev & Titarchuk 1974, Illarionov et al. 1979, T87, Grebenev & Sunyaev 1987, Magdziarz & Zdziarski 1995). We take into account contribution of the multiple scattering, using Fokker-Planck (diffusion) approximation and the first scattering exactly. This is a standard approach used in the classical radiative transfer theory for calculation of the coherent multiple scattering (e.g. Sobolev 1975).

The illumination of the semi-infinite atmosphere (disk) by the parallel flux  $\pi F(z)$  with inclination angle with respect to the disk normal  $\theta_0 = \cos^{-1}\mu_0$  produce the exponential primary photon distribution throughout the atmosphere as follows

$$f(\tau, z) = \frac{\lambda_\nu F(z)}{4} \exp(-\tau/\mu_0), \quad (22)$$

where  $\tau$  is the Thomson optical depth calculated from the upper disk surface. The first scattering component of the emergent spectral intensity observed at the angle  $\theta = \cos^{-1}\mu$  with respect to the disk normal is calculated by the integration of the primary photon distribution with the escape probability  $\exp(-\tau/\mu)/\mu$  along the line of sight (see, e.g., Chandrasekhar 1960)

$$I_1(\mu, \mu_0, z) = \frac{\lambda_\nu F(z)}{4} \frac{\mu_0}{\mu + \mu_0} \quad (23)$$

The multiple scattering component is produced by the integration of the Fokker-Planck (Kompaneets) equation and by integration of the product of its solution and the escape probability  $\exp(-\tau/\mu)/\mu$  along the line of sight.

The Fokker-Planck (Kompaneets) equation reads (T87, GS87)

$$\frac{1}{z^2} \frac{\partial}{\partial z} (\eta(z) z^2 n) + \frac{1}{3\phi(z)} \frac{\partial^2 n}{\partial \tau^2} - \frac{\sigma_A}{\sigma_T} n = -\frac{\lambda_\nu F(z)}{4} \exp(-\tau/\mu_0). \quad (24)$$

where  $n(z, \tau)$  is the photon occupation number,

$$\frac{\sigma_A}{\sigma_T} = 1 - \lambda_\nu \approx [Y + Y_0 \cdot \Theta(E - 7.11 \text{ keV})](7.8 \text{ keV}/h\nu)^3,$$

$$\phi(z) = (1 + 2.8z - 0.44z^2)^{-1}, \quad (25)$$

$$\eta(z) = \frac{z^2}{1 + 4.6z + 1.1z^2}. \quad (26)$$

The solution of this equation with the appropriate boundary condition at  $\tau_0 = 0$  ( $\partial n / \partial \tau - 3/2 = 0$ ) is given by the integral (T87, GS87)

$$J(\tau, z, \mu_0) = \frac{z}{4\eta(z)} \int_x^\infty \exp\left(-\int_z^{z_1} \frac{\sigma_A(t)}{\eta(t)\sigma_T} dt\right) \cdot \frac{\lambda_\nu F(z_1)}{z_1} dz_1 \int_0^\infty \exp(-\xi/\mu_0) P[\tau, u(z, z_1), \xi] d\xi. \quad (27)$$

where  $J(\tau, z, \mu_0) = z^3 n(\tau, z, \mu_0)$  is the average intensity,

$$P(\tau, u, \xi) = \frac{\sqrt{3}}{2\sqrt{\pi u}} \{ \exp[-3(\tau - \xi)^2/4u] + \exp[-3(\tau + \xi)^2/4u] - 3 \int_0^\infty \exp[-3(\tau + \xi + \eta)^2/4u - 3\eta/2] d\eta \}, \quad (28)$$

$$u(z, z_1) = \frac{1}{z} - \frac{1}{z_1} + 7.4 \ln(z_1/z) + 13.54(z - z_1), \quad (29)$$

$$\int_z^{z_1} \frac{\sigma_A(t)}{\eta(t)\sigma_T} dt = 3.375 \cdot 10^{-6} [Y + Y_0 \cdot \Theta(E - 7.11 \text{keV})] \cdot [0.25(z^{-4} - z_1^{-4}) + 1.53(z^{-3} - z_1^{-3}) + 0.55(z^{-2} - z_1^{-2})]. \quad (30)$$

Evaluation of the internal integral in equation (27) over  $\xi$  followed by the integration (over  $\tau$ ) of the product of the average intensity  $J(\tau, z, \mu_0)$  and the escape probability  $\exp(-\tau/\mu)/\mu$  along the line of sight gives us the multiple scattering component of the emergent spectral intensity

$$I_m(\mu, \mu_0, z) = \frac{z}{4\eta(z)} \int_x^\infty \exp\left(-\int_z^{z_1} \frac{\sigma_A(t)}{\eta(t)\sigma_T} dt\right) \frac{\lambda_\nu F(z_1)}{z_1} G[\mu, \mu_0, u(z, z_1)/3] dz_1. \quad (31)$$

where

$$G(\mu, \mu_0, t) = \frac{\mu_0}{(\mu^2 - \mu_0^2)(\mu_0 - 2/3)(\mu - 2/3)} [\mu_0(\mu^2 - 4/9)\varphi(t, \mu_0) - \mu(\mu_0^2 - 4/9)\varphi(t, \mu) + 2/3(\mu_0^2 - \mu^2)\varphi(t, 2/3)], \quad (32)$$

where  $t = u/3$  and

$$\varphi(t, \mu) = \text{erfc}(\sqrt{t}/\mu) \exp(t/\mu^2). \quad (33)$$

Thus, the final expression of the emergent spectral intensity is a sum of two components (eqs. [23] and [31])

$$I(\mu, \mu_0, z) = I_1(\mu, \mu_0, z) + I_m(\mu, \mu_0, z). \quad (34)$$

### 2.3.3 Spectral Properties of the Converging Inflow

As the optical depth of the flow becomes larger than 1, the momentum deposition by the bulk motion on the cooler soft photons becomes important (e.g. Blandford &

Payne 1981; Lyubarskii & Sunyaev, 1982). In the soft state, when the postshock region becomes cool and optically thick, the spectral properties would be dictated by this converging inflow.

The parameter which shows the importance of the bulk Comptonization effects relative to thermal Comptonization is  $\delta = 1/\Theta\dot{m}$ . For  $kT_e \ll m_e c^2$  and  $\dot{m} > 1$ ,  $\delta \gg 1$  and this leads to an asymptotic relation for the spectral index  $\alpha$

$$\alpha = 2\lambda^2 - 3.$$

Therefore, as long as  $\delta \gg 1$ , bulk Comptonization effects dominate and the values of  $\alpha$  are independent of the temperature of the electrons. For details of derivations of these parameters, see TMK96.

### 2.3.3.1 Spectral Index of Comptonization by Converging Inflow

In order to understand the origin of the hard component in converging inflow, one requires to solve an equation of the spectral energy flux  $F(r, \nu)$  with the boundary conditions of  $F \rightarrow 0$  at  $r \rightarrow \infty$ , and  $F = -0.5nx^3$  at the inner boundary:  $r \rightarrow 1$  (half the flux is absorbed by the hole). This boundary condition along with the radiative transfer equation imply that eigenvalue  $\lambda^2$  is the root of the equation

$$\left(\frac{5}{2} - \frac{2\lambda^2 - 3/2}{3}\tau_b\right)\Phi(-\lambda^2 + 5/2, 7/2, \tau_b) + \frac{5 - 2\lambda^2}{7}\tau_b\Phi(-\lambda^2 + 7/2, 9/2, \tau_b) = 0,$$

where  $\tau_b = 1.5\dot{m}$  and  $\Phi$  is the well known Kummer's function (e.g. Abramowicz & Stegun, 1964). In the limit of the large  $\dot{m}$ , the first root of this equation  $\lambda_1^2 = \lambda^2 \approx 2.25$  (TMK96) and thus  $\alpha = 1.5$ . Though this slope is obtained from Newtonian considerations, similar result is likely to remain valid even in general relativistic computation. This will be discussed elsewhere.

### 2.3.3.2 Luminosity and Effectiveness of Comptonization through Converging inflow

The relation between the luminosity of the low frequency photon source  $L_0 =$

$\int_0^\infty \delta(x - x_0)dx = 1$  and that of the source of hard radiation photons subjected to the converging inflow Comptonization ( $x = h\nu/kT_e$ ),

$$L = \int_0^\infty I(x)dx \quad (35)$$

is obtained using the integration technique developed in ST80, LS82, ST85,

$$E_{Comp} = \frac{L}{L_0} = \alpha(\xi - 1) \begin{cases} \frac{1}{\xi(\alpha - 1)} \left( 1 - \frac{\xi}{\xi + \alpha - 1} x_0^{\alpha-1} \right), & \text{for } \alpha \geq 1 \\ \frac{\Gamma(\xi)\Gamma(\alpha)\Gamma(1-\alpha)(1-x_0^{1-\alpha})x_0^{\alpha-1}}{\Gamma(\alpha+\xi)}, & \text{for } \alpha \leq 1 \end{cases} \quad (36)$$

where  $\xi = \alpha + 4 + \delta$ .

This is a generalization of ST80 results for the converging inflow case. Eq. (36) also has a continuous transition through spectral index  $\alpha = 1$  (see eq. 14).

The important conclusion from the above exercise is that the low-frequency source flux is amplified only by a factor of 3 ( $\alpha \sim 1.5$ ) due to Comptonization of the converging inflow into black hole. Thus the component is very weak and mainly visible in the soft state when either the postshock region is cold or when the shock is absent.

## 2.4 Solution Procedure

A fully self-consistent solution of the system shown in Fig. 1 involves the following considerations:

(1) The postshock region is hotter and thicker:  $h(r_s) \sim a_+(r_s)r_s^{3/2}$ ,  $a_+$  being the sound speed in the postshock region. It allows this region to intercept a fraction  $f_{ds}$  of the soft photons from the standard disk component. We compute self-consistently this intercepted soft component from each radial distance of the disk and integrate over the disk to obtain  $f_{ds}$ . This intercepted radiation is Comptonized in the postshock disk. From the two-temperature equations (eq. 6) we obtain electron temperature as a function of the optical depth. We then obtain an average electron temperature and the

enhancement factor following the prescription of ST85 and Titarchuk (1988, hereafter T88). In reality, we approximate the numerical averaging curves of ST85 and T88 by the following accurate analytical function (valid for spherical geometry):

$$g(\tau) = (1 - \frac{3}{2}e^{-(\tau_0+2)})\cos\frac{\pi}{2}(1 - \frac{\tau}{\tau_0}) + \frac{3}{2}e^{-(\tau_0+2)}$$

and obtain the average electron temperature from,

$$T_e(\tau_0) = \frac{\int_0^{\tau_0} T_e(\tau)g^2(\tau)(\tau_0 - \tau)^2d\tau}{\int_0^{\tau_0} g^2(\tau)(\tau_0 - \tau)^2d\tau}$$

Here,  $\tau_0$  is the total optical depth of the postshock region.

(2) After the computation of the Comptonization process, we calculate the fraction  $f_{sd}$  of this hard radiation that is intercepted by the standard disk. The interception is computed at each radial distance of the disk and then integrated over the whole disk. The rest  $(1 - f_{sd})$  of the hard radiation is directly radiated away to observers at infinity.

(3) We compute the albedo  $\mathcal{A}_\nu(r)$  of the preshock standard disk which determines the fraction of the intercepted flux scattered away at each radius of the disk. The rest  $\mathcal{B}_\nu(r) = 1 - \mathcal{A}_\nu(r)$  is assumed to be absorbed by the disk and is reradiated.

(4) In the zeroth order calculation, we assume that the equatorial Keplerian disk emits exactly as a standard Shakura-Sunyaev disk for  $r > r_s$ . After it absorbs a fraction  $f_{sd}\mathcal{B}_\nu(r)$  of the hard-radiation and reprocesses it, the temperature of the disk is computed at each radial distance.

We now give a simple argument why our algorithm (1-4) should converge: Let  $L_I = f_{ds}L_{SS}$  denote the fraction of the Shakura-Sunyaev (1973) disk luminosity  $L_{SS}$  of the soft radiation intercepted by the bulge of the shock,  $E_{Comp} = L_H/L_I$  denote the enhancement factor of this radiation due to cooling of the electrons through inverse Comptonization, and  $f_{sd}$  ( $\sim 0.25$  for a spherical bulge) denote the fraction of  $L_H$  intercepted back by the disk. The soft component observed from a disk around the black hole candidate is given by equation (2). The enhancement factor  $E_{Comp} \sim 3(T_e/3T_d)^{1-\alpha} \sim 10 - 30$



(for  $\alpha \sim 0.7 - 0.8$ ) because, typically, the electron temperature  $T_e \sim 50$  keV and the disk temperature  $T_d \sim 5$  eV for parameters of active galaxies and  $T_e \sim 150$  keV and  $T_d \sim 100$  eV for stellar black hole candidates. Hence, we easily achieve a convergence,  $f_{ds}E_{Comp}f_{sd}\mathcal{B}_\nu < 1$  since  $f_{sd} \sim 0.25$ ,  $f_{ds} \sim 0.05$ , and  $\mathcal{B}_\nu \sim 0.5$ .

In each run, we repeat steps (1) through (4) until the temperature distribution and the spectral index  $\alpha$  converges. Typically, 5 to 10 iterations are enough to achieve convergence.

### 3. RESULTS AND INTERPRETATIONS

In each case we compute, we choose a set of four quantities, namely, the mass of the central black hole  $M$ , the shock location  $r_s$  (instead of angular momentum of the halo), the accretion rate of the disk  $\dot{m}_d = \dot{M}_d / \dot{M}_{Edd}$  and the accretion rate of the halo  $\dot{m}_h = \dot{M}_h / \dot{M}_{Edd}$ . We shall present a series of runs for a galactic black hole candidate,  $M = 5M_\odot$ , and a series of runs when a black hole is massive,  $M = 10^7 M_\odot$ . In both the cases, we shall consider parameters suitable for a non-rotating black hole ( $r_s = 10r_g$ ,  $r_i = 3r_g$ ). By choosing two independent accretion rates, we thus do away with the unknown viscosity parameter.

In Fig. 2, we show the temperature distribution inside the disk and the postshock region when  $\dot{m}_d = 0.001$  (solid line), 0.01 (long-dashed line), 0.1 (short-dashed line) and 1 (dotted line),  $\dot{m}_h = 1$  is chosen throughout. We choose  $M = 5M_\odot$ . As the accretion rate of the Keplerian disk is increased, its temperature is increased. The postshock region, on the other hand, is *cooled*, since the number of soft photons intercepted by the postshock region is increased. The more the electrons cool through the inverse Compton process, the more the protons supply them energy through Coulomb coupling. Eventually, for  $\dot{m}_d = 1$ , the *runaway* process is seen where both the electrons and protons become cold catastrophically. Subsequently, the cooler but denser flow cools through the bremsstrahlung process alone. Exactly similar behavior is seen when the computation

around a massive black hole is also carried out.

If Comptonization is the dominant mechanism for cooling and the densities and velocities vary as in a spherical flow, i.e.,  $v \propto r^{-\frac{1}{2}}$  and  $\rho \propto r^{-\frac{3}{2}}$ , one can obtain an analytical expression for the electron temperature from the following equation (see, eq. [6]):

$$\frac{1}{T_e} \frac{dT_e}{dr} + \frac{1}{r} - C_{Comp} r^{1/2} \sim 0, \quad (37)$$

where  $C_{Comp}$  (obtainable easily from eq. [6]) is a monotonically increasing function of optical depth and the spectral index is assumed to be constant for a given case. The solution of the above equation is

$$T_e = \frac{T_{es} r_s}{r} e^{C_{Comp}(r^{3/2} - r_s^{3/2})}. \quad (38)$$

This shows that if  $C_{Comp} > r_s^{-3/2}$ , the cooling due to Comptonization overcomes compressional (geometric) heating and  $T_e$  drops as the flow approaches the black hole, and the convergent flow regime begins. Our numerical integration of equation (6) requires a somewhat higher amount of soft photons for cooling because of other heating effects, such as energy gain from the protons due to Coulomb process. The catastrophic cooling of the postshock region is important, since it introduces seed soft photons within the ‘convergent flow’ regime and produce the weaker hard component of slope  $\sim 1.5$ .

In Figure 3a, we present the variation of the energy spectral index  $\alpha$  (observed slope in the 2 – 50keV region) when a black hole of mass  $M = 5M_\odot$  is chosen. The abscissa is the logarithmic mass accretion rate of the Keplerian disk component ( $\dot{m}_d$ ) and the different curves are marked by the mass accretion rates of the halo component ( $\dot{m}_h$ ). We compared the results from the postshock flow as well as the convergent inflow. The dashed curves are drawn where the spectra could be contaminated by both effects. In Fig. 3b, we show mean electron temperature. The solid curve is for  $\dot{m}_h = 1.0$  and the long-dashed and short-dashed curves are for  $\dot{m}_h = 2.0$  and 0.5 respectively. For a given halo rate, a transition between states can be achieved by a change in  $\dot{m}_d$ . Qualitatively,

the cooling rate due to Comptonization for unit optical depth is proportional to the electron temperature and the local energy density, i.e.,  $L_H/\tau_h \propto T_e(L_H + L_I)$ . Hence,  $\tau_h T_e \propto (1 + L_I/L_H)^{-1}$ . In the hard state,  $L_I \ll L_H$  and  $\tau_h T_e \sim \text{constant}$ . When  $\tau_h \lesssim 1$ , this leads to  $\alpha \sim \text{constant}$  (T94, TL95, see also, Pietrini & Krolik, 1995). This is what we observe as well:  $\alpha$  is insensitive to the  $\dot{m}_d$  when  $\dot{m}_d \lesssim 0.1$ . In the soft state,  $L_I \gg L_H$  and  $T_e \sim \frac{L_H}{L_I} \frac{1}{\tau_h}$ . Smaller  $T_e$  leads to a very high  $\alpha$ , as observed. For a smaller  $\dot{m}_h$ , the optical depth  $\tau_h$  becomes small and the temperature high, causing the index to become especially sensitive to both  $\dot{m}_d$  and  $\dot{m}_h$ . When accretion rate of the disk is very high, the spectral index asymptotically becomes 1.5, as is observed in many systems (e.g. Sunyaev et al. 1994, Miyamoto et al. 1991, Parmar et al. 1993, Wilson & Rothschild 1983). Successful fits of soft spectra of black hole candidates GS1124-68 (Ebisawa et al., submitted) and GRS1009-45 (Titarchuk et al., submitted) have been obtained using our model. These fits are therefore consistent with a freely-falling, sub-Keplerian component close to a black hole.

In Figures 4(a-b), we present the same quantities computed for a massive black hole ( $M = 10^7 M_\odot$ ) candidate. The results are similar, though the average temperature is smaller and the index  $\alpha$  is more sensitive to the disk rate when  $\dot{m}_d \gtrsim 1$  and  $\dot{m}_h \gtrsim 1$ . Here, the rapid rise of  $\alpha$  is due to the abrupt cooling (see Fig. 2) of the postshock region within a narrow layer.

Figure 5 shows the contribution of the component spectra for a particular case with  $\dot{m}_d = 0.1$ ,  $\dot{m}_h = 1.0$ ,  $M = 5M_\odot$ . For illustration, the observation angle  $\theta$  is chosen so that  $\mu = \cos\theta = 0.4$ . The long dashed curve represents the soft spectrum from the Keplerian disk, while the short dashed curve is the contribution to the soft spectrum from the reprocessed and intercepted hard radiation by the Keplerian disk (second term in eq. [2]). The dotted curve is the contribution to the hard radiation from the postshock region. The dash-dotted curve denotes the reflected hard radiation from the Keplerian disk. The sum of these contributions is depicted by the solid curve.

Figure 6 shows a comparison of the four runs for the spectra around a black hole of mass  $5M_{\odot}$  and  $\dot{m}_h = 1.0$ . The disk accretion rates ( $\dot{m}_d$ ) are 0.001 (solid line), 0.01 (long-dashed line), 0.1 (short-dashed line) and 1.0 (dotted line) respectively. As shown in Figs. 3a, 3b, 4a, 4b, with the increase of the disk accretion rate, the temperature  $T_e$  of the electrons is reduced and the energy index  $\alpha$  is increased. The luminosity and the peak frequency of the soft component go up monotonically with  $\dot{m}_d$ . The hard component shows a ‘pivoting’ property: the intensity of the hard component rises with  $\dot{m}_d$  below  $\nu \sim 10^{18-19}$  Hz (corresponding energy  $\sim 5 - 50$  keV) but it falls at higher energies since the electrons become cooler. In the soft state, the postshock region becomes cooler and produces a weak hard component of slope ( $\alpha \sim 1.5$ ) due to the convergent flow as shown by the dash-dotted curve. In Fig. 7 we show this ‘power-law’ feature with the components separated. The long-dashed curve is the soft-luminosity from the Keplerian accretion disk and the short-dashed curve is due to the Comptonization of the intercepted ( $\sim 5\%$ ) soft photons in the convergent flow. This power-law component is possibly the only true signature of black hole and is observed in black hole candidate spectra (e.g. Sunyaev et al. 1994). In the neutron star case, the flow need not pass through the inner sonic point (C89, C90a,b) if it is not compact enough and the flow is subsonic at the surface. Thus, no significant bulk momentum is added to the soft photons to create this hard component. Indeed, in this case, turbulent mixing of halo and disk components in the postshock region becomes important, which results in a hard component of slope  $< 1$  and electron temperature  $T_e \sim 12$  keV which is observed (Claret et al. 1994).

If the angular momentum of the overall disk, or even the sub-Keplerian component, is quite low,  $l \ll l_{ms}$ , the disk need not have a shock at all. Shock free advective disk (originating out of Keplerian component, see, Appendix) can also intercept soft photons from the Keplerian disk and show similar behaviors mentioned here. It is unclear whether X-ray emitted in this process would be efficient. As the viscosity of the disk varies, the sub-Keplerian flow would meet the Keplerian disk at varying distance (Appendix, C95b) and could mimic the hard-to-soft state transition. However, in this

case soft and hard components would always be correlated which is not observed.

Increasing the halo rate  $\dot{m}_h$  increases the optical depth of the postshock region thereby increasing the hard component luminosity  $L_H$ . The spectrum is hardened due to the saturation of Comptonization (see, Figs. 3a and 3b). Figures 8a and 8b show the comparison of electron temperatures (in K) and the spectra, respectively, as  $\dot{m}_h$  is varied while  $\dot{m}_d = 0.1$  is kept fixed throughout. Solid, long-dashed, and short-dashed curves are drawn for  $\dot{m}_h = 1, 2$  and  $0.5$  respectively. Contrary to what is observed in Fig. 6, the hardening of the spectra in the present circumstance is accompanied by no significant change in the soft luminosity and an actual *increase* in the hard luminosity.

The above computations use the shock location to be  $r_s \sim 10r_g$  and the inner edge at  $3r_g$ . These are the typical length scales for accretion of matter with marginally stable angular momentum (C89, C90a,b). An increase in angular momentum of the halo increases the location of the shock, cools the average postshock electron temperature and raises the average spectral index. It also suppresses the soft luminosity relative to the hard luminosity. Similarly, a study of the behavior in the Kerr geometry with, say,  $r_s = 5r_g$  and  $r_i = 1.5r_g$  with similar disk and halo parameters indicates a general increase of the average halo temperature and an average decrease of the spectral index.

The above mentioned properties from our model are summarized (see also, CTKE95) in Table 1 where the correlation (arrows pointing up) or anticorrelation (arrows pointing down) of the observable quantities (luminosities  $L_{X,\gamma}$  in X-ray and  $\gamma$ -ray regions) with the input accretion rates are shown. Smaller arrows represent a weaker correlation.

TABLE 1

Variations of the Spectral Properties with Accretion Rates

	<i>Input</i> $\rightarrow$	$\dot{m}_d$	$\dot{m}_h$
Output $\downarrow$	Row & Column	(1)	(2)
$L_S$	(1)	$\uparrow$	$\uparrow$
$L_X, \alpha$	(2)	$\uparrow\uparrow^a$	$\uparrow\downarrow^{b,c}$
$L_\gamma, \alpha$	(3)	$\downarrow\uparrow^a$	$\uparrow\downarrow^b$

<sup>a</sup> dependence is weaker for  $\dot{m}_d \lesssim 0.1$ <sup>b</sup> dependence is weaker for  $\dot{m}_h \gtrsim 1$ <sup>c</sup>  $\alpha_X \sim 1 \rightarrow 1.5$ ,  $L_X/L_S \leq 10^{-3}$  in the convergent flow regime (see, Fig. 3)

## 4. COMPARISON OF THE PREDICTED BEHAVIOR WITH OBSERVATIONS

So far, we have delineated the spectral properties of the accretion disks which are formed out of Keplerian and sub-Keplerian matter. We can now compare these predictions with the observed facts. Galactic black hole candidates, such as *GX339-4*, *GS2023+338* and *GS1124-68* show almost constant spectral slopes over two decades of the luminosity variation. (TAN; Ueda et al. 1994, hereafter U94; E94). The constancy of the slope is explained by the lower left corner of Fig. 3a. The spectral evolution of the black hole candidate novae, *GS2000+25*, *GS2023+338*, and *GS1124-68* are very different (TAN; E94). These differences could be accounted for by variations of the

properties of the halo (Figs. 8a and 8b). For instance, *GS2023+338* is always in the hard state throughout the outburst, suggesting a high  $\dot{m}_h > 1$  but lower  $\dot{m}_d \lesssim 0.01 - 0.1$ . The suppression of the soft component could also be due to a distant shock. *GS2000+25*, on the other hand, remained in the soft state during the outburst, suggesting a high  $\dot{m}_d \sim 1.0$ , but a low  $\dot{m}_h \lesssim 0.1 - 0.5$ . In the rising phase of *GS1124-68* (E94), the increase of  $L_H$  below  $\sim 10$  keV is accompanied by its decrease above  $\sim 10$  keV. This is the ‘pivoting’ property in the hard spectra we referred to (Fig. 6). This object, along with other black hole candidates such as *Cyg X-1* and *GX339-4* are observed in two distinctly different states. Generally speaking, in the hard state,  $\alpha \sim 0.7$  remains almost constant but in the soft state the hard component is very weak with index  $\alpha \sim 1.0 - 1.5$ , again remaining constant during a the period in which  $L_S$  varied by as much as two orders of magnitude (TAN, E93, E94). In the soft state,  $\dot{m}_d$  is very high and the postshock optically thick region produces a spectral index of  $\sim 1.5$  as it would in a convergent flow (Fig. 6). In *GS2023+338*, the tendency of the anticorrelation between  $L_X$  and  $L_\gamma$  is also seen (TAN, Sunyaev et al., 1991), but they do not actually cross, possibly because both  $\dot{m}_d$  and  $\dot{m}_h$  change together. The hard component in galactic black hole candidates is generally found to be more variable than the soft component and the variations are found to be on time scales of days to months (TAN, I92, E94). This is possibly due to independent variations in accretion rates as we have chosen in our model.

Among the massive black hole candidates associated with AGNs, *NGC 4151* has been studied extensively (Yaqoob 1992; Yaqoob et al. 1993). *NGC 4151* shows  $\alpha$  to be generally stable though it is seen to rise with the hard luminosity in the 2 – 20keV range. This is consistent with our result of variation of  $\dot{m}_d$  (Fig. 6) where we show that below the pivoting, the hard luminosity rises with  $\alpha$ . The  $\alpha$ - $L_H$  plot also showed some scatter. This can be understood from our Fig. 8b, where we show that when the halo rate is increased, the hard flux increases with the decrease of  $\alpha$ . Because of longer time-scales, Seyferts do not show a change of states. We believe that possibly all Seyfert-1s belong to different regions of the same diagram (Figures 4a and 4b). A

spectral index of  $\sim 1.5$  is also reported in MKN841 (Arnaud et al., 1986) whose origin could be the same as that of the galactic black holes discussed above.

## 5. CONCLUDING REMARKS

In this paper, we have presented the spectral properties of the accretion flows which are primarily sub-Keplerian or an admixture of Keplerian and sub-Keplerian at the outer boundary. Such matter produces an optically thick standard disk on the equatorial plane and the sub-Keplerian optically thin halo surrounding it produces a shock close to the black hole or a neutron star. We showed that the reprocessing of the soft-photons from the standard disk by the hotter, postshock region of the disk is sufficient to produce the observed hard radiation with correct behavior of the luminosity and the spectral slope. We showed that the spectral index  $\alpha \sim 0.7-0.8$  could remain generally stable even when the accretion rate of the disk ( $\dot{m}_d$ ) is changed by more than 2 orders of magnitude, as long as  $\dot{m}_d \lesssim 0.1$ . This is seen in objects such as, *GX339-4*, *GS2023+338* and *GS1124-68* and possibly in some class of Seyferts. When the disk accretion rate is close to the Eddington rate, the sensitivity of  $\alpha$  to the accretion rate goes up and the object switches to the soft state as the disk accretion rate is increased. We also showed that during the change of the state, the hard luminosity remains the same in some energy band, a property (pivoting) that is observed in GS1124-68. Usually, this location of the pivoting depends upon the accretion rate. A search for this property in a wide band ( $2 - 200\text{keV}$ ) should be made in other black hole candidates, such as Cyg X-1 and GX339-4 to verify our model. A similar property is expected in X-ray bursters, and other neutron star candidates as well. We also showed that in the soft state, the consideration of the convergent flow becomes applicable. We believe that the spectral slope of 1.5 that is seen in the soft state is the signature of a very large converging flow close to the black hole. For a neutron star accretion, such a component should clearly be absent. Traces of convergent inflow should be observable at very high energies even in hard state, since the halo rate remains high.



It may be possible that for stellar black holes, the two components of the disk, namely, the sub-Keplerian and the Keplerian, are of different origin. The sub-Keplerian component may be from the winds, whereas the Keplerian component is primarily from the surface of the companion. If they were of same origin (i.e. from a completely Keplerian or a sub-Keplerian disk), the variation at the source would be reflected in the variation of the hard and the soft components at two different times. This is because the halo is almost freely falling, whereas the disk is moving on a viscous timescale. Roughly speaking, for a similar halo and disk thickness variation with radius, the ratio of the time scales would be  $t_{disk}/t_{halo} \sim 1/\alpha_v$ , where  $\alpha_v$  is the Shakura-Sunyaev viscosity parameter (Shakura & Sunyaev 1973) inside the disk. However, even this correlation may be generally difficult to detect, since, whereas the variation of the disk rate changes both the soft and the hard luminosities, the variation of halo rate changes primarily the hard component. Also, the variation of the hard flux and the spectral index are inversely correlated with these rates (Figs. 6 and 8b). Another source of complexity could be the entrainment and evaporation of some disk matter which joins the halo and the loss of some matter as winds and outflows. Details of these processes can be quantitatively understood through numerical simulations and will be discussed elsewhere.

We have noted above that there could be two sources of strong winds in the vicinity of the disk. Numerical simulations show that centrifugal barrier pushes sub-Keplerian, inviscid flows along the direction of the jets (Hawley et al. 1984, 1985; Eggum, Coroniti, & Katz, 1987; MLC94, Ryu et al. 1995). Another source of winds could be the evaporation of matter close to the shock. Judging from the resemblance of the iron resonance line shapes (Piro, Yamauchi, & Matsuoka, 1990; Rajeev et al. 1994; Mushotzky et al. 1995) with the P-Cygni profiles and the profiles of down-scattered emission lines we believe that these lines could be generated from the winds themselves. These profiles are characterized by the prominent emission feature at the red wing and by possibly weaker absorption feature at the blue wing. We are more convinced by the fact that we find the upper limit of the equivalent width of the lines from the disk to be only about a few tens of electron volts, as opposed to the observed equivalent width of

several hundreds of electron volts. A back-of-the-envelope calculation for the ionization parameter (Kallman & McCray 1982) could be done using typical parameters for the wind. This turns out to be,  $\xi = L_H|_{7-10\text{keV}}/n_p r^2 \sim 10^4 (\frac{\dot{m}_h}{\dot{m}_w})_2 (\frac{v}{c})_{0.1}$  where,  $n_p$  is the number density of protons and  $\dot{m}_w$  is the outflow rate of the line driven wind in units of the Eddington rate. Here, a tenth of velocity of light (subscript 0.1) and a 50% of loss in halo matter (subscript 2) are assumed. The column density  $N = 3.5(\dot{m}_h)_1 (\frac{v}{c})_{0.1}^{-1} (\frac{r_{in}}{20r_g})^{-1} \text{ g cm}^{-2}$  may be sufficient to produce the observed iron line in the outflow. The subscript 1 of  $\dot{m}_h$  indicates that one Eddington rate is assumed. The emergent spectrum of the outflow is a result of transmission of the injected hard radiation. Fig. 9 shows the fate of this hard component (with a typical  $\alpha \sim 0.7$  for illustration) when it passes through a wind of  $\tau \sim 3$ . The solid curve shows the emitted component from the postshock region and the long-dashed curve is the component down-scattered (ST80) by the outflow (for energy change by down scattering, see, eq. 17). The short-dashed curve is produced due to the absorption by heavy elements at the outer layer of the outflow (pronounced iron edge is seen). We do not include the line emissions. If the so-called “reflection bump” originates in the wind, as we suggest, the net effect must be a combination of the solid and the short-dashed curve weighted appropriately by the covering factor. In computing the effect of reflection, it is well known that only a finite layer of an otherwise semi-infinite target participates in scattering. Thus, the *continuum* spectra from these two approaches (namely, from reflection and transmission) are indistinguishable. However, the equivalent width of the emitted lines should be higher in the outflow, because of a larger (by an order of magnitude or so) covering factor. The equivalent width of the lines and the strength of our “transmission bump” should be correlated as they both depend on the covering factor. In the rotating winds and outflows, splitted emission lines should be generated. Such observations are reported in Tanaka (1994) and Tanaka et al. (1995). High optical depth ( $\tau > 3$ ) of the disk components close to the hole washes out any disk emission features and thus these lines can only be emitted from the winds. Down scattering mimics gravitational red-shifts of lines. Thus the line profiles in these two processes are again indistinguishable, apart from the sharp cut-off in the red wing when a disk emission is considered.

Combining results presented in Fig. 1, Fig. 3 and Fig. 10, we are now in a position to construct sequences of a nova outburst and its quiescent state (e.g., Cannizzo, 1993). In the quiescent state, entire disk has low viscosity and the Keplerian disk recedes very far away (Fig. 10). As the viscosity in the equatorial plane rises, Keplerian disk rate is increased, and the inner edge of the Keplerian component comes closer to the black hole. This increases soft photons to be Comptonized, thereby generating an outburst. This situation is to be compared with an atomic reactor whose energy output is controlled by insertion of the fuel rods (here, the Keplerian disk component) by varying degree.

In our model we have made some approximations, such as the equations appropriate for conical geometry (instead of actual torus) to integrate both the Euler equations as well as the radiative transfer equations. Also, we assumed a fixed polytropic index rather than computing it self-consistently from the heating and cooling as the flow accretes. We have ignored diffusion of hard photons to the preshock region and subsequent pre-heating of the electrons, as is the characteristics of the photo-hydrodynamical shocks (Riffert, 1988; Becker 1988). However, we do not believe that our basic conclusions will be affected by these approximations.

It is to be noted that our model differs significantly from the Comptonized soft photon model of two-temperature hot disks discussed almost two decades ago (Shapiro, Lightman, & Eardley 1974; Shakura & Sunyaev 1976). In these models, the soft and the hard radiations originate from the same disk and therefore, the variations of the hard and the soft components should be always correlated, this does not appear to be observed. There are some other models in the literature (Wandel & Liang 1991; Haardt & Maraschi 1991) which required extra-components and/or extra parameters. Our present model is somewhat more general than the single component model (which included shock waves) of Chakrabarti & Wiita (1992) where only the optical and UV regions were considered.

If the shock waves do exist, as we assumed in our model, there could be another

manifestation which is observable as well. Recently Molteni, Sponholz, & Chakrabarti (1996) have shown that when the accretion rates are such that the cooling time scale roughly matches the infall time scale, the shock oscillates with a time period comparable to the cooling time. Could this be the origin of quasi periodic oscillations (QPOs) seen in black hole candidates (e.g., Dotani 1992) such as GX339-4 and GS1124-68? Possibly, yes. Particularly noteworthy is the fact that by dynamically moving back and forth, the shocks modulate the outgoing hard radiation by as much as 10 to 15 percent, whereas the soft radiation emitted from the preshock disk is only marginally modulated. This is because of the fractional variation of the emitting area is larger for the postshock region. These behaviors have been observed in dwarf novae, such as SS Cygni, VW Hyi, and U Gem (see, e.g., Mauche, Raymond, & Mattei, 1995). Unlike the case of a dwarf novae outburst, where cooling could be due to bremsstrahlung or line effects, in the black hole candidates, the time scale is governed by Comptonization processes.

Though we have primarily discussed shock waves around a galactic or extragalactic black holes, the entire computation remains unchanged when a neutron star is considered instead. The typical size of a neutron star (10 km) is under  $2.5r_g$  and therefore our computation zone ( $3-10r_g$ ) is outside that of a neutron star. For example, the best fit of the hard spectra of the burst source MXB 1728-34 by a Comptonization model (ST80) requires the parameters  $kT_e = 12$  keV and the optical depth  $\tau_0 > 3.8$  (Claret et al. 1994) which are easily achievable by our model with a disk and a postshock boundary layer. Though it may be generally difficult to distinguish the spectral properties of a galactic Schwarzschild black hole from that of a neutron star, we believe that the hard component due to the convergent flow (Fig. 6) is possible only in a black hole accretion since the inner boundary conditions are completely different (C89, C90a,b).

Works of SKC and LGT are partially supported by the National Research Council and NASA grant No. NCC5-52, respectively. The authors thank D. Kazanas, K. Ebisawa, T. Yaqoob and T. Kallman for useful discussions. They also thank Paul Wiita for carefully reading the manuscript and suggesting improvements.

# APPENDIX

The globally complete viscous, isothermal solutions around a black hole are in C90a,b where sub-Keplerian flows become Keplerian at large distance. In this Appendix, we show this even in the presence of general heating and cooling.

We choose a simple, vertically averaged, axisymmetric, polytropic disk. The equations governing the flow are (C95a,b):

(a) The radial momentum equation:

$$v \frac{dv}{dr} + \frac{1}{\rho} \frac{dP}{dr} + \frac{l_{Kep}^2 - l^2}{r^3} = 0, \quad (A.1a)$$

(b) The continuity equation:

$$\frac{d}{dr}(\rho r h v) = 0, \quad (A.1b)$$

(c) The azimuthal momentum equation:

$$v \frac{dl(r)}{dr} - \frac{1}{\rho r h} \frac{d}{dr} \left( \frac{\alpha P r^3 h}{\Omega_{Kep}} \frac{d\Omega}{dr} \right) = 0 \quad (A.1c)$$

(d) The entropy equation:

$$\Sigma v T \frac{ds}{dr} = Q^+ - Q^- \quad (A.1d)$$

These equations are the generalization of viscous, transonic, isothermal disks for which the global solutions are already in the literature (C90a,b). Here  $l_{Kep}$  and  $\Omega_{Kep}$  are

the Keplerian angular momentum and Keplerian angular velocity respectively,  $\Sigma$  is the density  $\rho$  vertically integrated,  $P$  is the total pressure,  $h$  is the vertical thickness of the disk at radial distance  $r$ ,  $v$  is the radial velocity,  $s$  is the entropy density of the flow,  $Q^+$  and  $Q^-$  are the heat gained and lost by the flow. We compute  $h(r)$  assuming the disk is in hydrostatic balance equation in vertical direction.  $l(r)$  is the angular momentum distribution of the disk matter. Here, we have chosen geometric units, thus  $r$  is units of Schwarzschild radius  $r_g = 2GM/c^2$ ,  $l(r)$  is in units of  $2GM/c$ , and velocities are in units of the velocity of light  $c$ ,  $M$  being the mass of the central black hole. To mimic the black hole geometry (i.e., to compute the Keplerian quantities above) we use Paczyński-Wiita (1980) potential. In eq. (A.1c),  $\alpha_v \lesssim 1$  in the above equation is the viscosity parameter of Shakura & Sunyaev (1973), which is widely used to describe the viscous stress:  $w_{r\phi} = -\alpha P$ . Eqn. A.1c could be easily integrated to obtain the disk angular momentum distribution.  $l(r) - l(r_{in}) = \alpha_v r a^2 / v$  (C90a,b). Without any loss of generality, we assume  $Q_-$  to be a fraction of  $Q_+$  while integrating above equations. Also, in order that the angular momentum remains continuous across shock waves, we choose total pressure (thermal plus ram) in the viscosity prescription (CM95). One needs to supply five quantities (over-determined system, since we are not explicitly computing the heating and coolings to illustrate our point here): the angular momentum at the inner edge  $l(r_{in})$ , the location of the inner sonic point  $r_c$ , the viscosity parameter  $\alpha_v$ , the polytropic index  $\gamma = 4/3$  and the cooling law  $Q_-/Q_+$ .

Fig. A.1 shows examples of the ratio of the disk angular momentum distribution to the Keplerian distribution (for  $r < 3r_g$ , we keep  $l_{Kep}(r) = l_{Kep}(3r_g)$  for stability reasons) as a function of distance from the black hole. The ratios show deviation from Keplerian due to advection, pressure and viscous effects. Three diverse cases have been chosen to illustrate our points. In Case A (marked ‘A’), we choose  $l(r_{in}) = 1.88$ ,  $r_c = 2.2$ ,  $\alpha_v = 0.005$ ,  $\gamma = 4/3$  (radiation pressure dominated) and  $Q_- = Q_+$ . The flow deviated from Keplerian disk at  $7.5r_g$  and even becomes super-Keplerian (ratio  $> 1$ ) close to the black hole. In Case B (marked ‘B’), we choose  $r_c = 2.3$ ,  $l(r_{in}) = 1.7$ ,  $\gamma = 5/3$  (gas pressure dominated),  $\alpha_v = 0.02$  and  $Q_- = Q_+$ . Here the flow deviates

from Keplerian at  $90r_g$  and always remained sub-Keplerian. In both the cases above, there is no shock formation. In Case C (marked ‘C’), the flow passes through a shock at  $13.9r_g$  (angular momentum distribution remained continuous) and remains completely sub-Keplerian after deviating from the Keplerian disk at  $480r_g$ . The parameters chosen are  $l(r_{in}) = 1.6$ ,  $r_c = 2.87$ ,  $\gamma = 4/3$ ,  $\alpha_v = 0.05$  and  $Q_- = 0.5Q_+$ . It is easily shown that a decrease of viscosity, keeping other parameters fixed, increases the distance where Keplerian disk begins. This property is crucial in understanding our model of the generalized disk (Fig. 1) and the nova outbursts.

## REFERENCES

- Abramowitz, M., & Stegun, I.A. 1964, Handbook of Mathematical Functions, U.S. Dept. of Commerce, Washington. D.C.
- Abramowicz, M., Czerny, B., Lasota, J.P., & Szuszkiewicz, E., 1988, ApJ, 332, 646
- Arnaud, K. et al. 1985, MNRAS, 217, 105
- Basko, M.M. 1978, ApJ, 223, 268
- Basko, M.M., Sunyaev, R.A., & Titarchuk, L.G. 1974 A&A, 31, 249
- Becker, P., 1988, ApJ, 327, 772
- Blandford, R.D. & Payne, D.G. 1981, MNRAS, 194, 1033
- Cannizzo, J.K., 1993 in *Accretion Disks in Compact Stellar Systems*, ed. J. Craig Wheeler (Singapore: World Scientific), 6.
- Chakrabarti, S.K. 1989, ApJ, 347, 365 (C89)
- Chakrabarti, S.K. 1990a, MNRAS, 243, 610 (C90a)
- Chakrabarti, S.K. 1990b, Theory of Transonic Astrophysical Flows (Singapore: World Scientific, Singapore, 1990) (C90b)
- Chakrabarti, S.K. 1993, Numerical Simulations in Astrophysics, Eds. J. Franco et al. (Cambridge Univ. Press: Cambridge) (C93)
- Chakrabarti, S.K. 1994, in Proceedings of the 17th Texas symposium, (New York Academy of Sciences, New York)
- Chakrabarti, S.K. 1995a, in Accretion Processes on Black Holes, Physics Reports (in press) (C95a)
- Chakrabarti, S.K. 1995b, ApJ Letters, submitted, (C95b)
- Chakrabarti, S.K., & Molteni, D. 1995, MNRAS, 272, 80 (CM95)
- Chakrabarti, S.K., Titarchuk, L., Kazanas, D., & Ebisawa, K. 1995, A&A Suppl. Ser., Proceedings of 3rd Compton Symposium (CTKE95)
- Chakrabarti, S.K., & Wiita, P.J. 1992, ApJ, 387, L21
- Chandrasekhar, S. 1960, Radiative Transfer, (New York: Dover)
- Chen, X. M., & Taam, R. 1993, ApJ, 412, 254
- Chen, X. M., Abramowicz, M., Lasota, J.P., Narayan, R. & Yi, I. 1995, ApJ, 443, L61
- Clavel, J. et al. 1990, MNRAS, 246, 668
- Claret, A. et al. 1994, ApJ, 423, 436



- Done, C. et al. 1992, ApJ, 395, 375
- Dotani, Y, 1992 in *Frontiers in X-ray Astronomy*, (Tokyo: Universal Academy Press ), 152
- Ebisawa, K. et al. 1993, ApJ, 403, 684 (E93)
- Ebisawa, K. et al. 1994, PASJ, 46, 375 (E94)
- Eggum, G.E., Coroniti, F.V., & Katz, J.I. 1987, ApJ, 323, 634
- Grebenev, S.A., & Sunyaev, R.A. 1987, Sov. Astron. Lett. 13, 438
- Haardt, F. et al., 1993, 411, L95
- Haardt, F., & Maraschi, L., 1991, ApJ, 380, L51
- Hawley, J.F., Smarr, L.L., & Wilson, J.R. 1984, ApJ, 277, 296
- Hawley, J.F., Smarr, L.L., & Wilson, J.R. 1985, ApJS, 55, 211
- Hua, X., & Titarchuk, L.G. 1995, ApJ, 449, 188 (HT95)
- Illarionov, A.F., Kallman, T., McCray, R., & Ross, R.R. 1979, ApJ. 228, 279
- Inoue, H. 1992, in *Frontiers of X-ray Astronomy*, ed. Y. Tanaka & K. Koyama, (Tokyo: University Press), 291 (I92)
- Kallman, T.R., & Krolik, J. H. 1986, ApJ., 308, 805
- Kallman, T. R., & McCray, H. 1982, ApJ Supp. Ser, 50, 263
- Liang, E.P., & Thompson, K.A. 1980, ApJ, 240, 271
- Lang, K.R., 1980, *Astrophysical Formula*, (Springer Verlag, New York)
- Lybarskii, Yu.E., & Sunyaev, R.A. 1982, Soviet Astr. Lett. 8, 330
- Magdziarz, P. & Zdziarski, A.A., 1995, MNRAS, 273, 837
- Malkan, M. 1982, ApJ, 254, 22
- Mauche, C.W., Raymond, J.C., & Mattei, J.A. 1995, ApJ (in press)
- Molteni, D., Sponholz, H., & Chakrabarti, S.K. 1995, ApJ (submitted)
- Molteni, D., Lanzafame, G., & Chakrabarti, S.K. 1994, ApJ, 425, 161 (MLC94)
- Muchotrzeb, B., & Paczyński, B. 1982, Acta Astron. 32, 1
- Miyamoto, S. et al. 1991, ApJ, 383, 784 Narayan, R., & Yi, I. 1994, ApJ, 428, L13
- Novikov, I., & K.S. Thorne. 1973. in: *Black Holes*, eds. C. DeWitt and B. DeWitt (Gordon and Breach, New York)
- Paczynski B., & Bisnovaty-Kogan, G. 1981, Acta Astron. 31, 283

- Paczynski B., & Wiita, P.J. 1980, A&A, 88, 23
- Parmar, A.N. et al. 1993, A&A, 279, 179 Perola, G.C. et al. 1986 ApJ, 306, 508
- Peterson, B.M. et al. 1991 ApJ, 368, 119
- Pietrini, P., & Krolik, J.H. 1995, ApJ, in press
- Piro, L., Yamauchi, M., & Matsuoka, M. 1990, ApJ, 360, L35
- Rajeev, M.R., Chitnis, V.R., Rao, A.R. & Singh, K.P. 1994, ApJ., 424, 376
- Rees, M.J., Begelman, M.C., Blandford, R.D. & Phinney, E.S. 1982, Nat, 295, 17
- Riffert, H. 1988. ApJ, 327, 760
- Ryu, D., Brown, G., Ostriker, J., & Loeb, A. 1995, ApJ, (in press)
- Shakura, N.I., & Sunyaev, R.A. 1973, A&A, 24, 337
- Shakura, N.I., & Sunyaev, R.A. 1976, MNRAS, 175, 613
- Shapiro, S.L., & Teukolsky, S.A., Black Holes, White Dwarfs and Neutron Stars, 1984 (John Wiley & Sons: New York)
- Sobolev, V.V., 1975, Light Scattering in Planetary Atmosphere (Pargamon Press: Oxford)
- Sunyaev, R.A. et al., 1991, Astron. Lett., 17, 123
- Sunyaev, R.A. et al., 1994, Astron. Lett., 20, 777
- Sunyaev, R.A. & Titarchuk, L.G. 1980, A&A, 86, 121 (ST80)
- Sunyaev, R.A. & Titarchuk, L.G. 1985, A&A, 143, 374 (ST85)
- Sun, W.H. & Malkan, M. 1989, ApJ, 346, 68
- Shapiro, S.L., Lightman, A.P., & Eardley, D.M., 1974, ApJ, 204, 187
- Tanaka, Y., 1989, in the *Proceedings of the 23rd ESLAB symposium*, ed. J. Hunt & B. Battrock vol. 1, p.3 (Paris:ESA) (TAN)
- Tanaka, Y. 1994, in *New Horizons of X-ray Astronomy*, eds. F. Makino & T. Ohashi (Tokyo: Universal Academy Press)
- Tanaka, Y. et al. 1995, Nat., 375, 659
- Titarchuk, L.G. 1987, Soviet Astrofizika, 26, 57 (Astrophysics 1988, 26, 97) (T87)
- Titarchuk, L.G. 1988, Soviet Astrofizika, 29, 634 (Astrophysics 1988, 26, 97) (T88)
- Titarchuk, L.G. 1994, ApJ, 434, 570 (T94)
- Titarchuk, L.G., & Lyubarskij, Yu 1995, ApJ, in press (TL95)

- Titarchuk, L.G., Mastichiadis, A. & Kylafis, N., 1996, ApJ, submitted (TMK96)
- Ueda, Y., Ebisawa, K., & Done, C., 1994, PASJ, 46, 107
- Wandel, A., & Liang, E.P., 1991, ApJ, 380, 84
- Wilson, C.K. & Rothschild, R.F. 1983, ApJ, 274, 717 Yaqoob, T., 1992, MNRAS, 258, 198
- Yaqoob, T. et al., 1993, MNRAS, 262, 435
- Zdziarski, A.A. et al. ApJ, 363, L1 1990

## FIGURE CAPTIONS

Fig. 1: Schematic diagram of the accretion processes around a black hole. An optically thick, Keplerian disk which produces the soft component is surrounded by an optically thin sub-Keplerian halo which terminates in a standing shock close to the black hole. The postshock flow Comptonizes soft photons from the Keplerian disk and radiates them as the hard component. Iron line features may originate in the rotating winds.

Fig. 2: Proton and electron temperatures ( $T_p$  and  $T_e$  in  $^{\circ}\text{K}$ ) inside the disk and the postshock region when  $\dot{m}_d = 0.001$  (solid line), 0.01 (long-dashed line), 0.1 (short-dashed line) and 1 (dotted line). Other parameters are  $\dot{m}_h = 1$  and  $M = 5M_{\odot}$ . At higher accretion rates, the postshock region cools faster and the convergent flow regime begins.

Fig. 3(a-b): Variation of the (a) energy spectral index  $\alpha$  (observed slope in the 2–50 keV region) and (b) the mean electron temperature (in keV)  $T_e$  as functions of the disk and halo accretion rates. Notice the stability of  $\alpha$  in the hard state and the transition of states when  $\dot{m}_d \sim 0.1 - 1.0$ .  $M = 5M_{\odot}$  is chosen. Halo rates are marked on the curve. In (a), computed spectral index in soft states due to convergent flow is also provided. Dashed curves indicate regions where both components could contribute. In (b), short-dashed, solid and long-dashed curves are for halo rates 0.5, 1.0 and 2.0 respectively.

Fig. 4(a-b): Same as Figs. 3a and 3b except that  $M = 10^7 M_{\odot}$  is chosen. In this case, the average electron temperature is generally lower, and the spectral index generally higher.

Fig. 5: Contributions of various components to the net spectral shape (solid). Long dashed, short dashed, dotted and dash-dotted curves are the contributions from the Shakura-Sunyaev disk  $r > r_s$ , the reprocessed hard radiation by the Shakura-Sunyaev

disk, reprocessed soft-radiation by the postshock disk  $r < r_s$  and the hard radiation reflected from the Shakura-Sunyaev disk along the observer ( $\mu=0.4$ ). The contribution of the preshock halo which is orders of magnitude lower is ignored. Parameters are  $\dot{m}_d=0.1$ ,  $\dot{m}_h=1$ , and  $M=5 M_\odot$ .

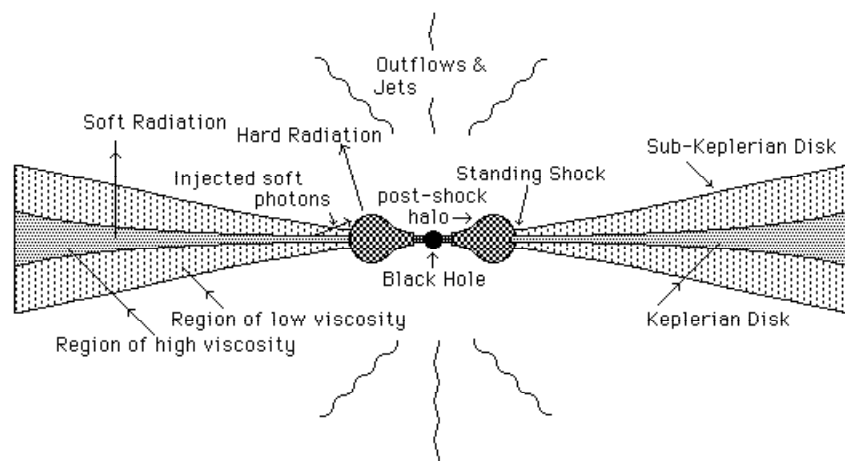
Fig. 6: Variation of the spectral shape as the accretion rate of the disk is varied.  $\dot{m}_d=0.001$  (solid line), 0.01 (long-dashed line), 0.1 (short-dashed line), and 1 (dotted line). Though the soft luminosity increases with  $\dot{m}_d$ , the hard luminosity may show ‘pivoting’ or crossing as intermediate energies. Note the correlation and anticorrelation of the hard flux and the spectral index before and after the pivoting point. The dash-dotted curve represents the hard component from convergent inflow near the black hole and has the characteristics of the slope  $\sim 1.5$  in soft state.

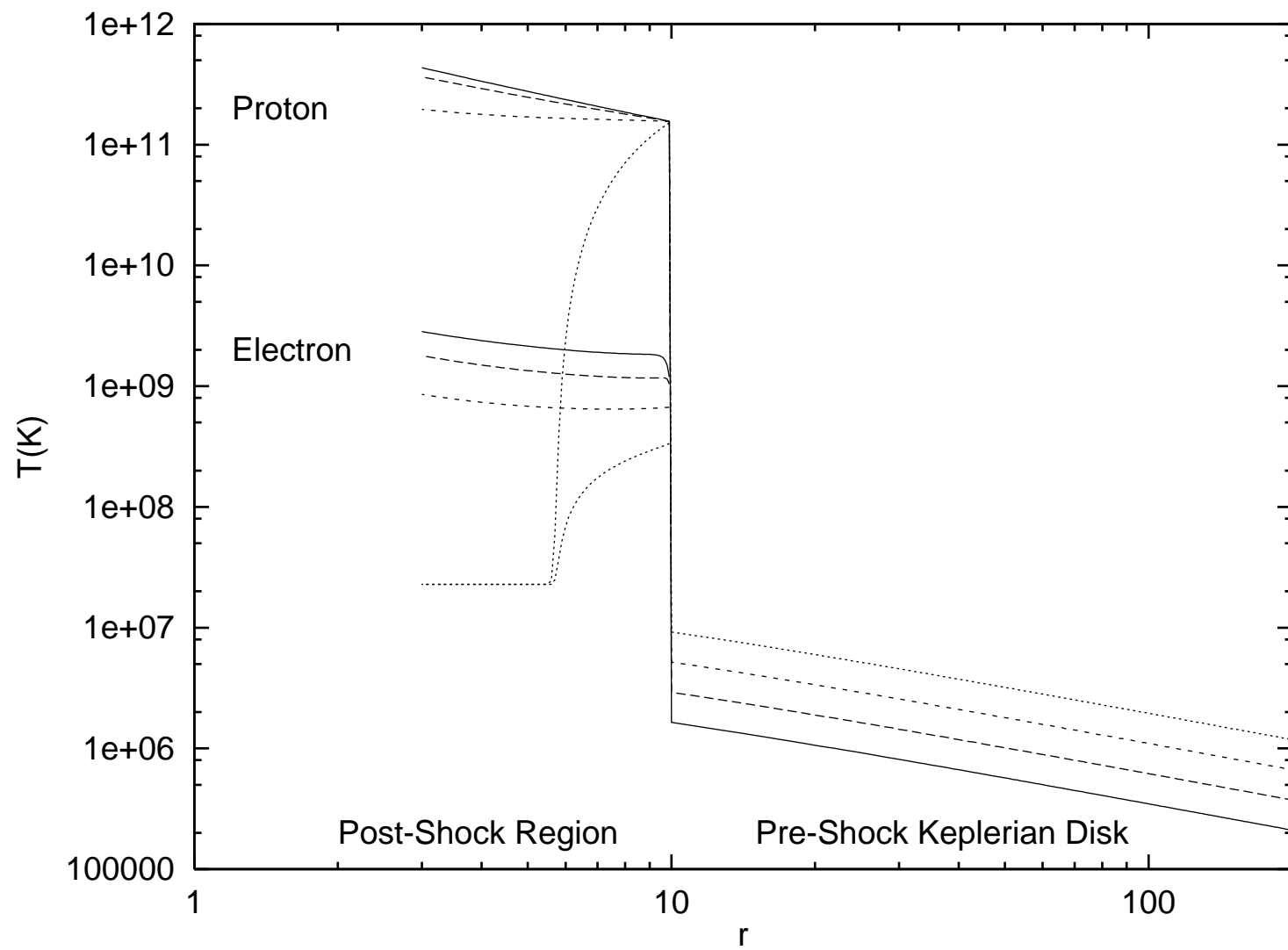
Fig. 7: Spectral shape of a Keplerian disk with a very high disk accretion rate. The postshock region cools immediately due to Comptonization and the cooler photons are subsequently Comptonized by momentum deposition from the converging bulk motion close to the black hole. The spectral slope is  $\alpha \sim 1.5$ , an universal feature of black hole candidates in the soft state.

Fig. 8(a-b): Variation of the (a) temperature (in  $^{\circ}\text{K}$ ) and (b) spectral shape as the accretion rate of the halo is changed.  $\dot{m}_h=1$  (solid),  $\dot{m}_h=2$  (long dashed) and  $\dot{m}_h=0.5$  (short dashed). The hard flux goes up but the spectrum hardens with  $\dot{m}_h$  while the disk temperature and the soft luminosity remain virtually unchanged.

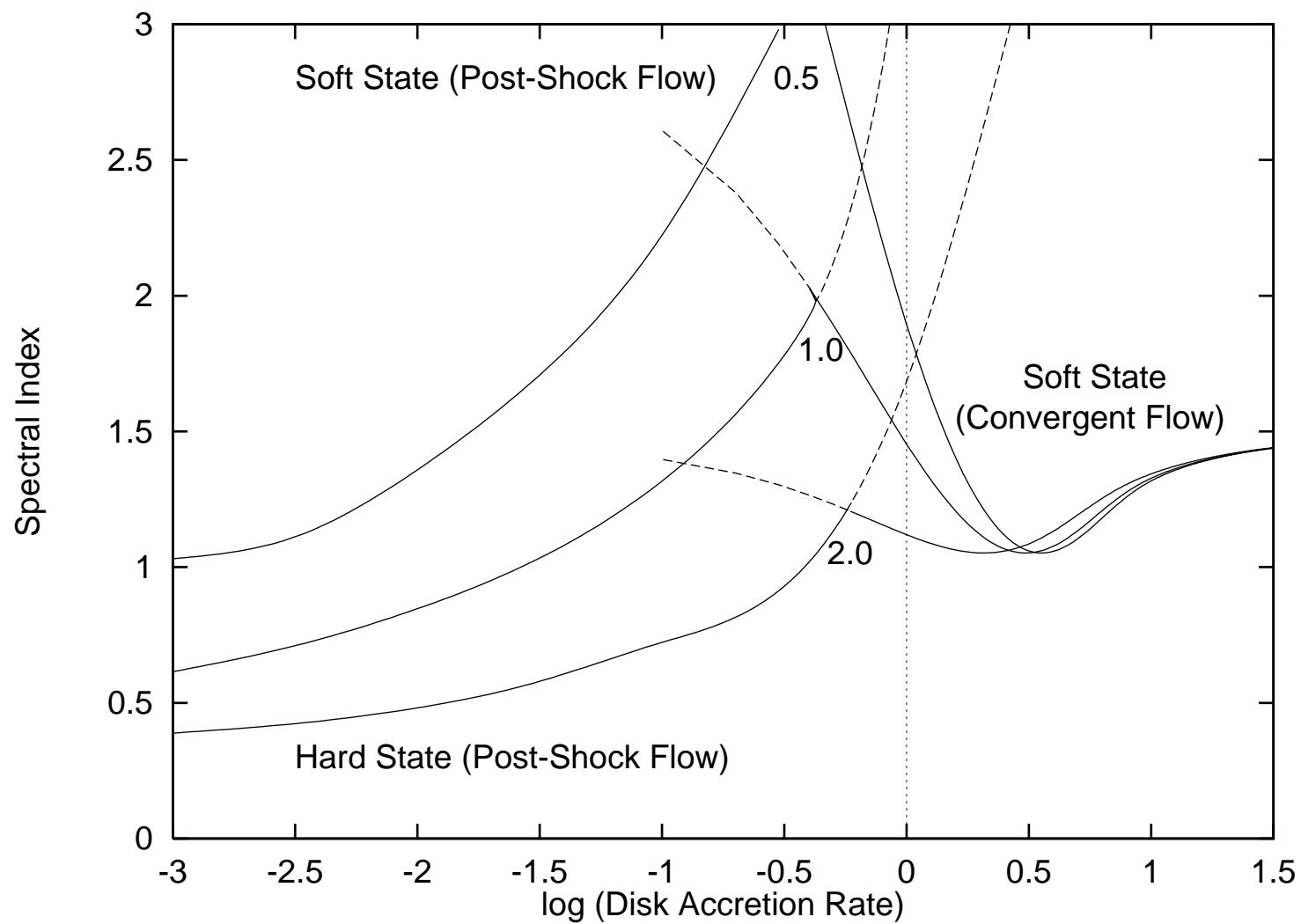
Fig. 9: Fate of a power-law hard component in presence of a wind of  $\tau \sim 3$  with a hundred percent converging factor. Emitted (solid line), down-scattered component (long-dashed line) and its absorption by the cooler outer region (short-dashed line) are shown. This “transmission bump” from the wind is indistinguishable from the “reflection bump” from the disk, except for the higher equivalent width in the former case.

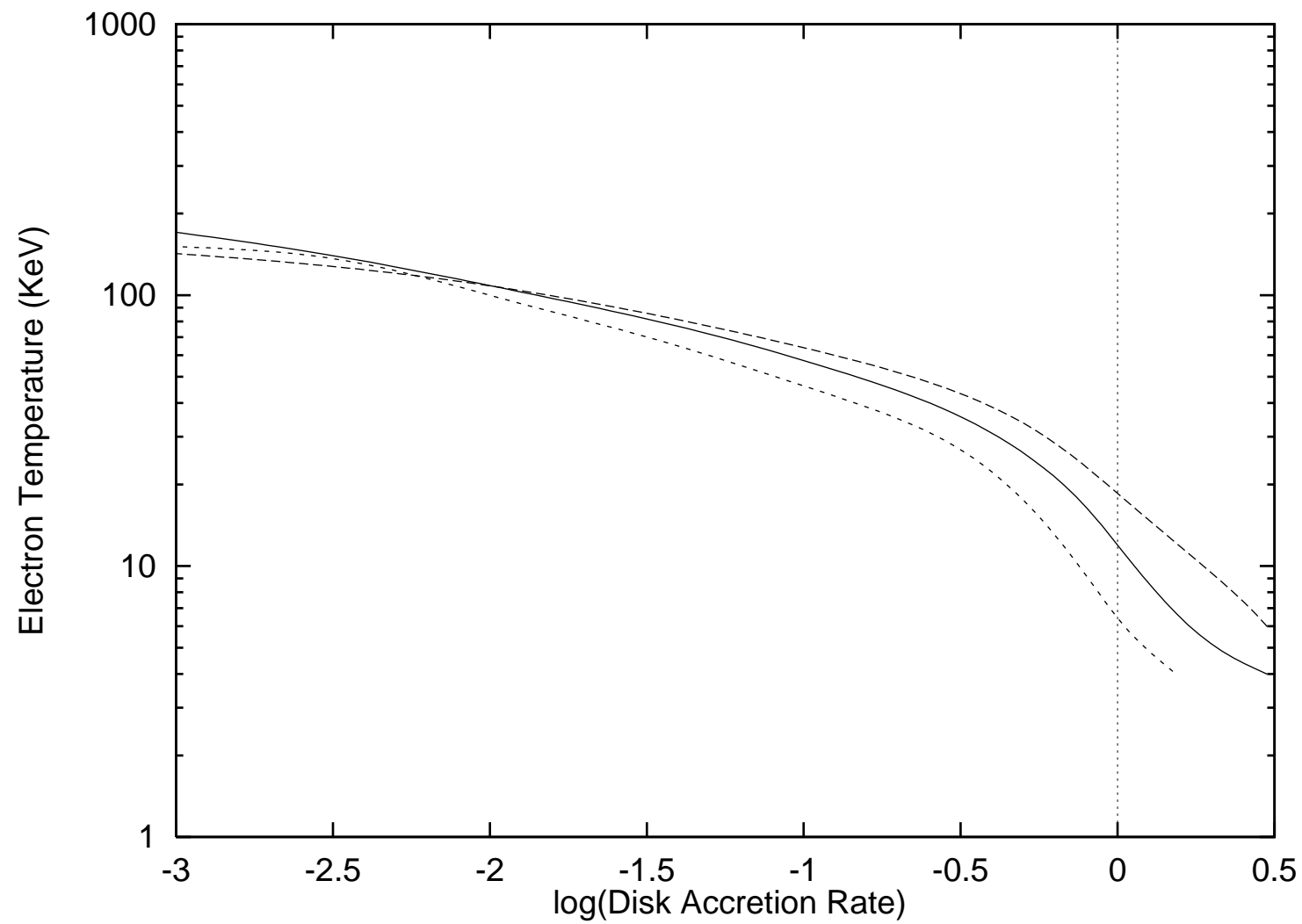
Fig. 10: Ratio of the disk angular momentum to Keplerian angular momentum in three different cases. In case marked ‘A’, the flow becomes sub-Keplerian before becoming super-Keplerian close to the black hole. In case marked ‘B’, the disk becomes sub-Keplerian and remained so before entering the black hole. In case marked ‘C’, the disk becomes Keplerian, then passed through a standing shock at  $r = 13.9r_g$  before entering the black hole.

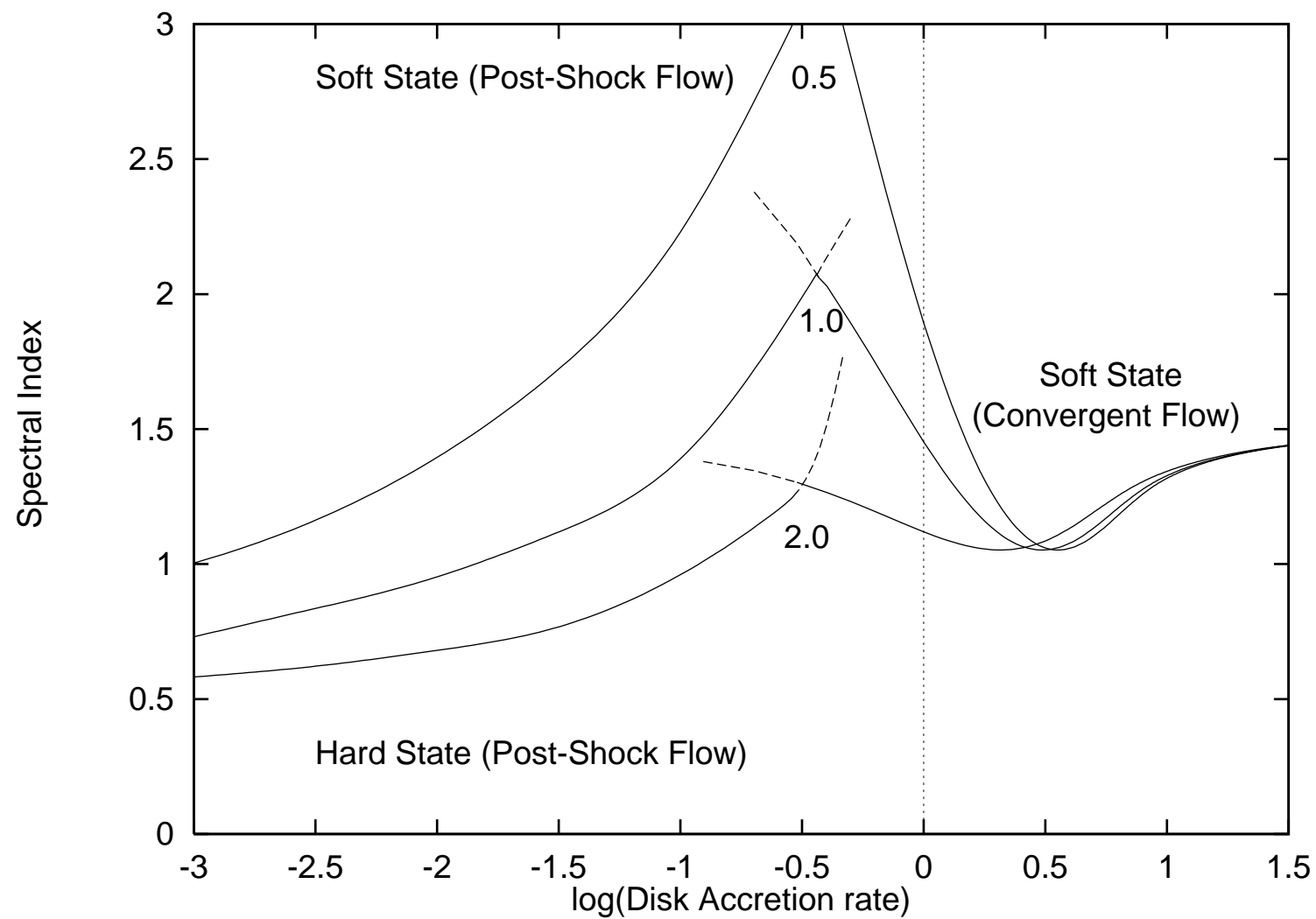


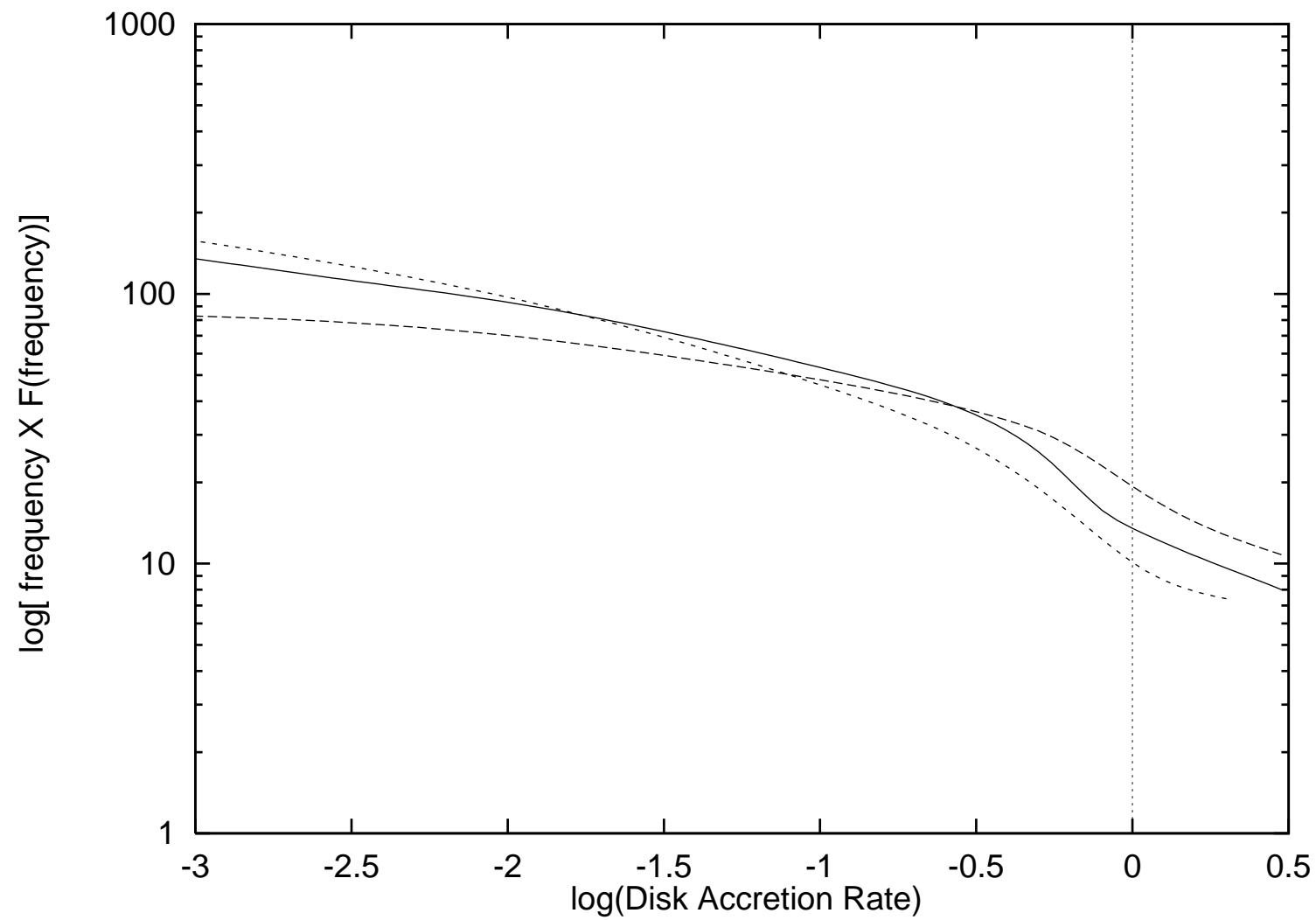


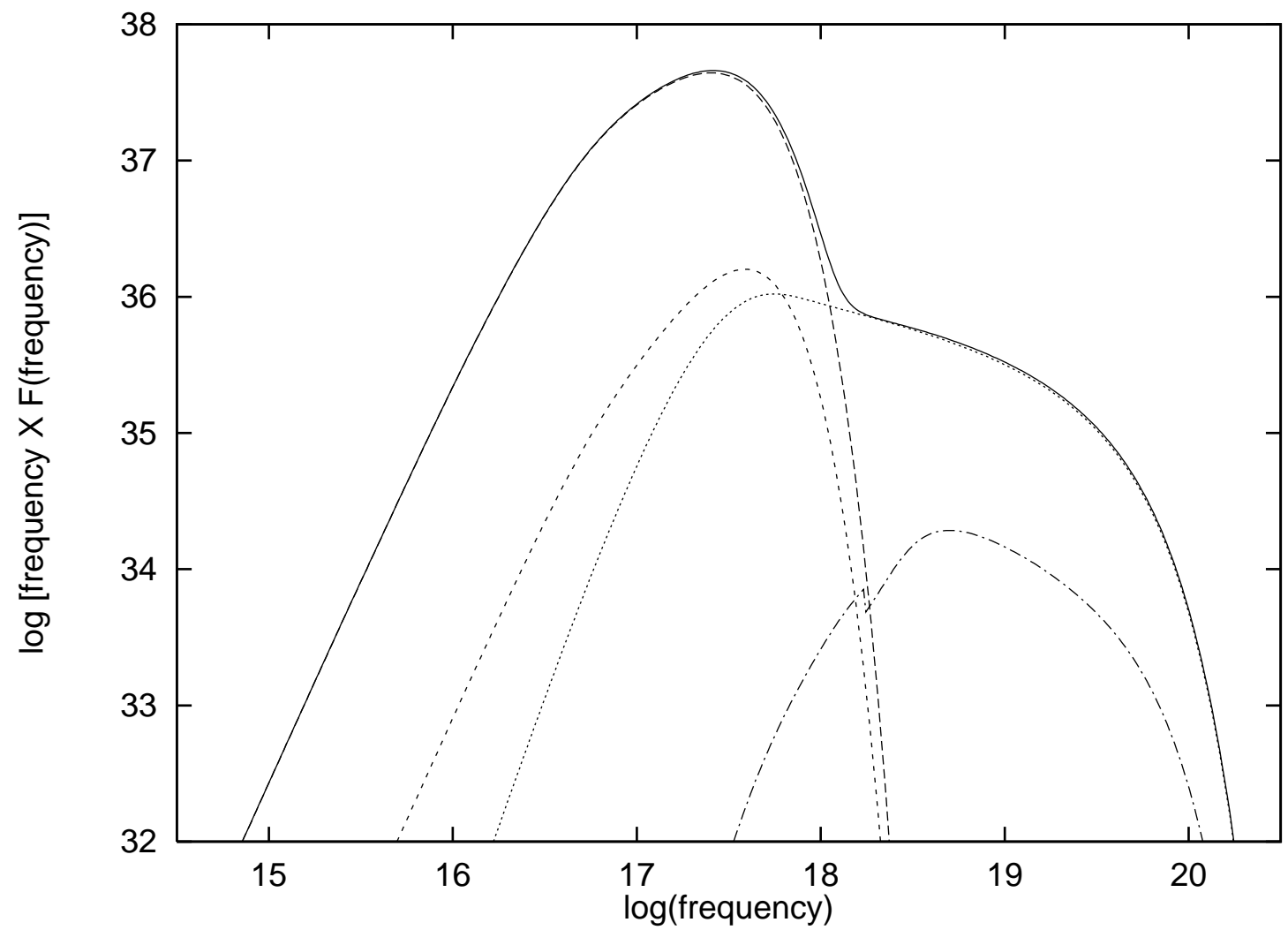


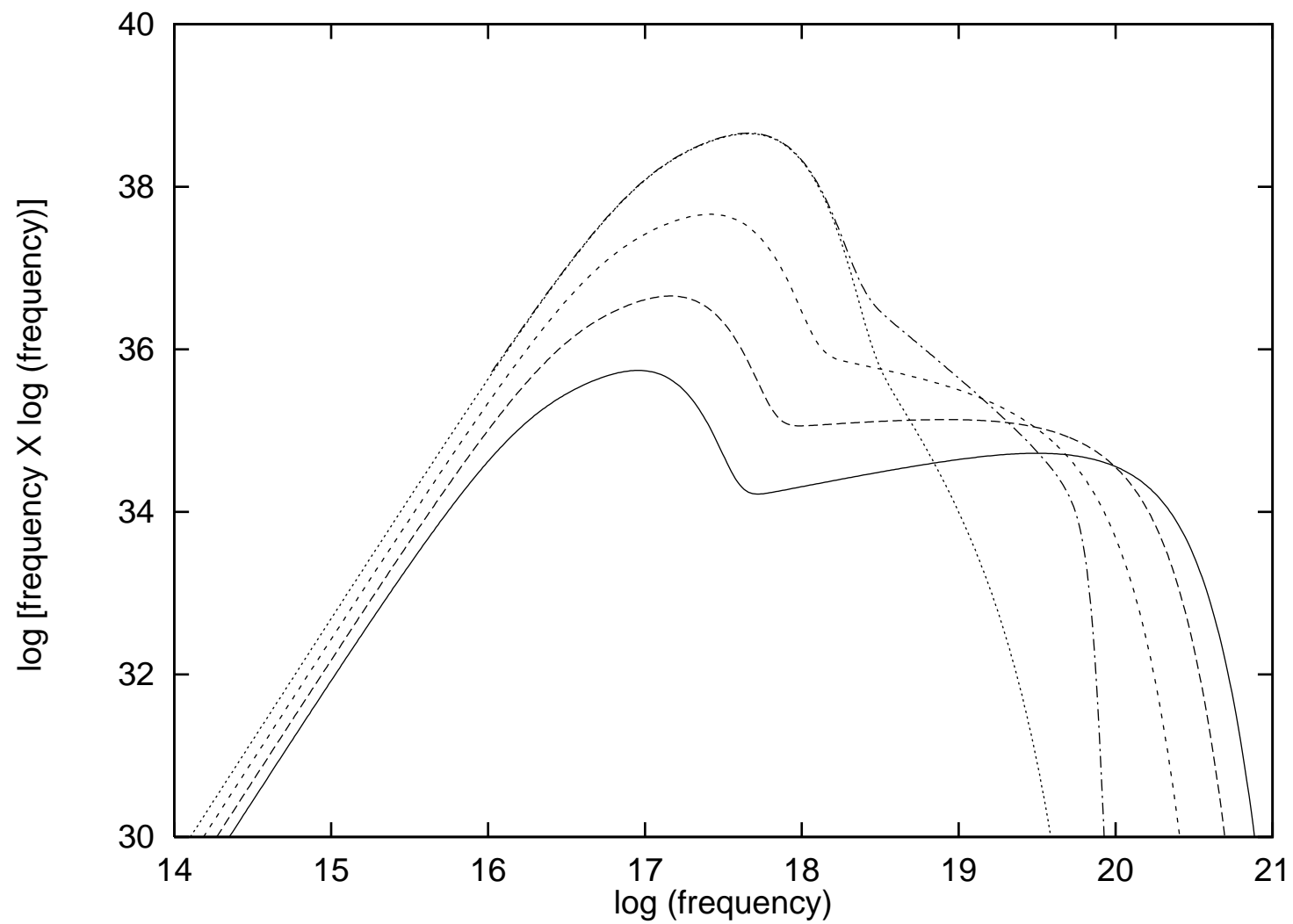


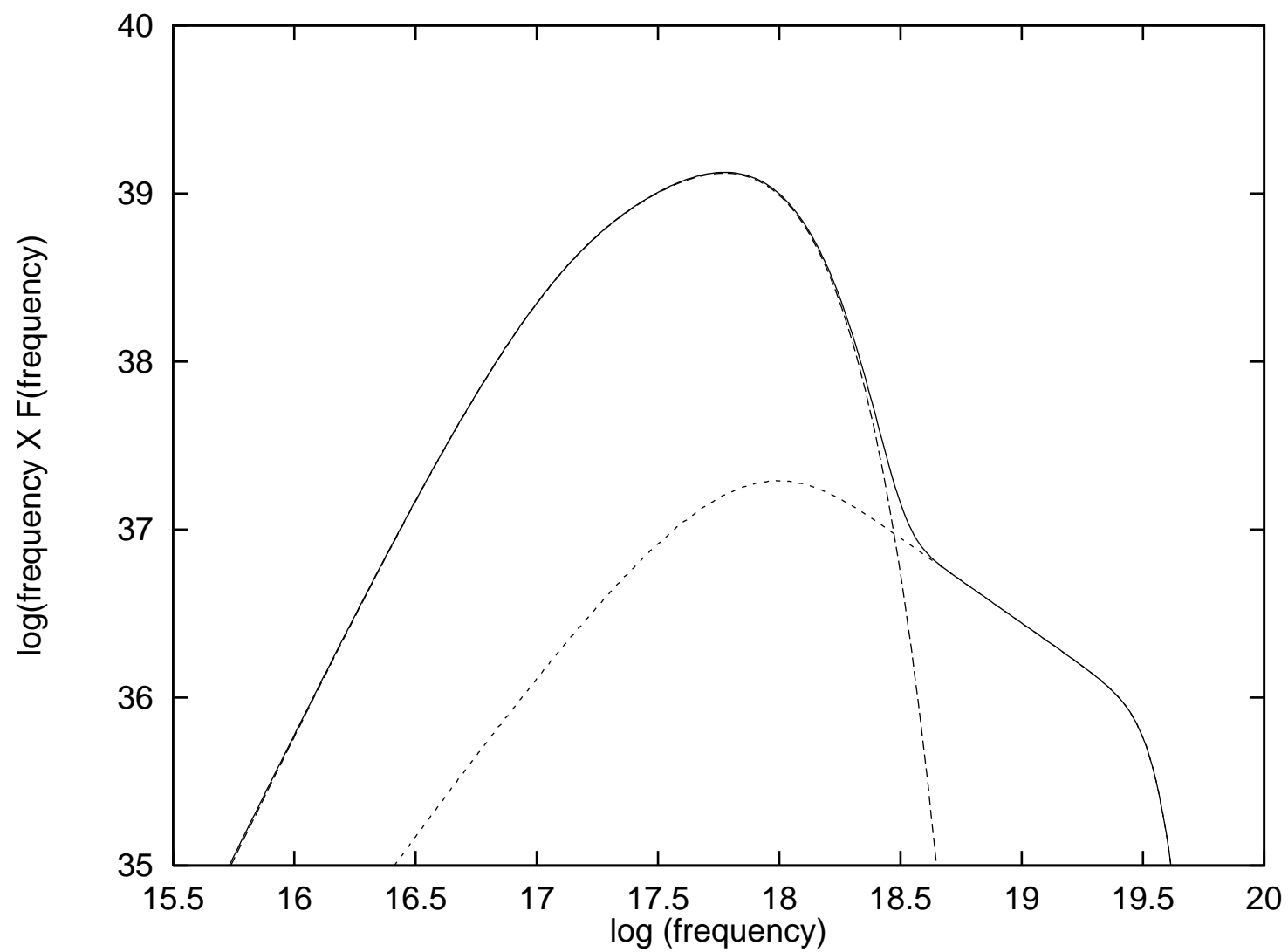


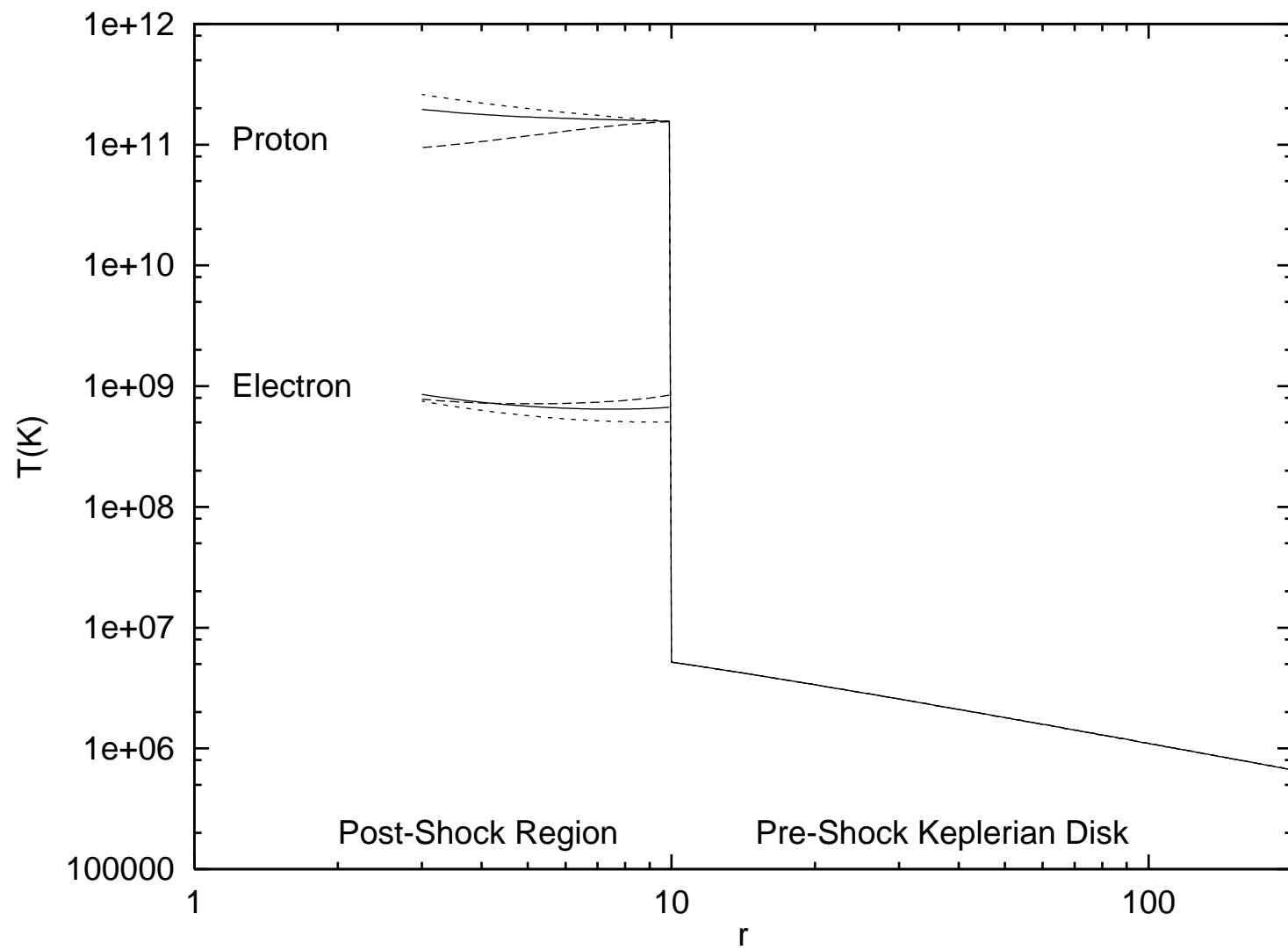




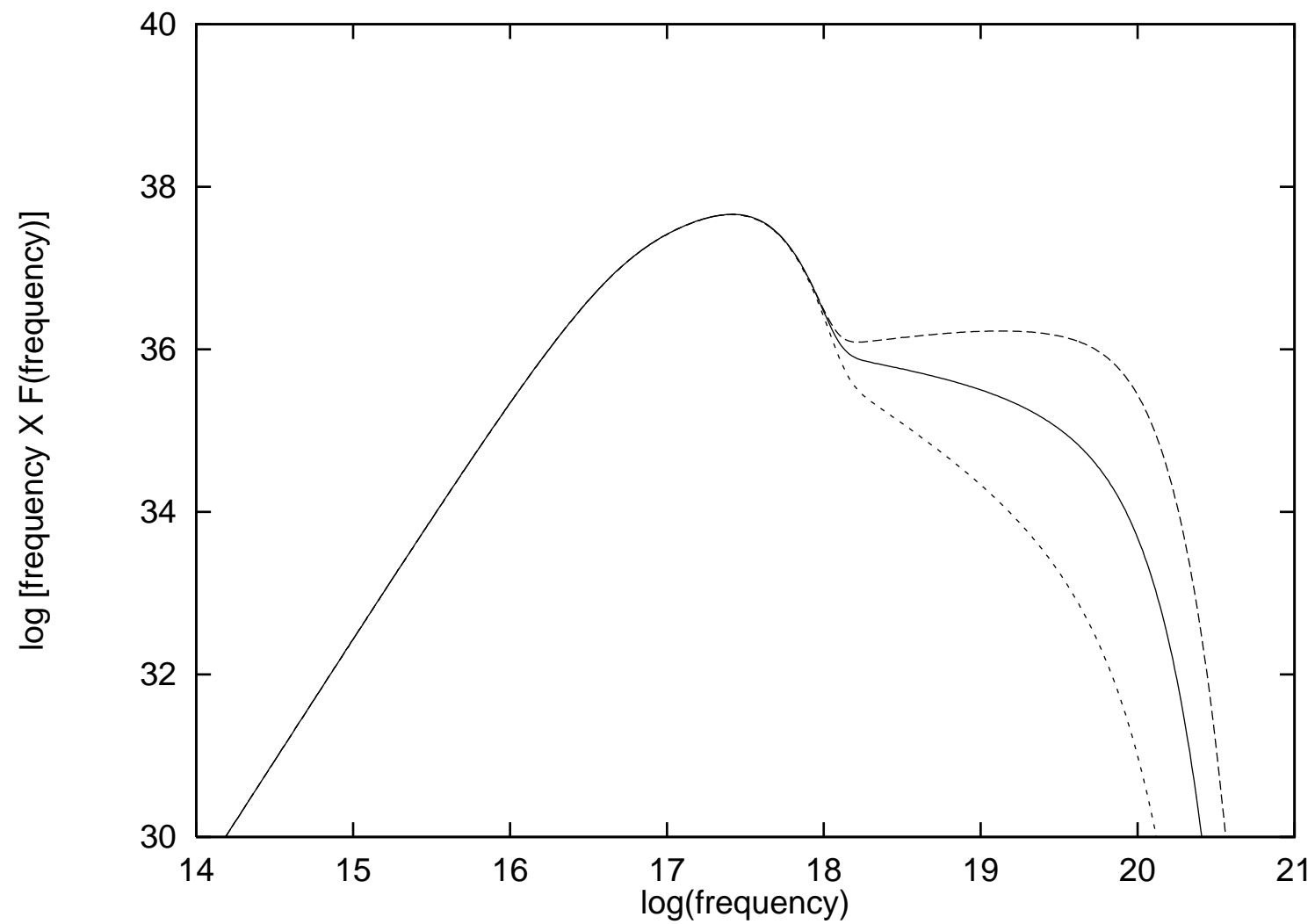


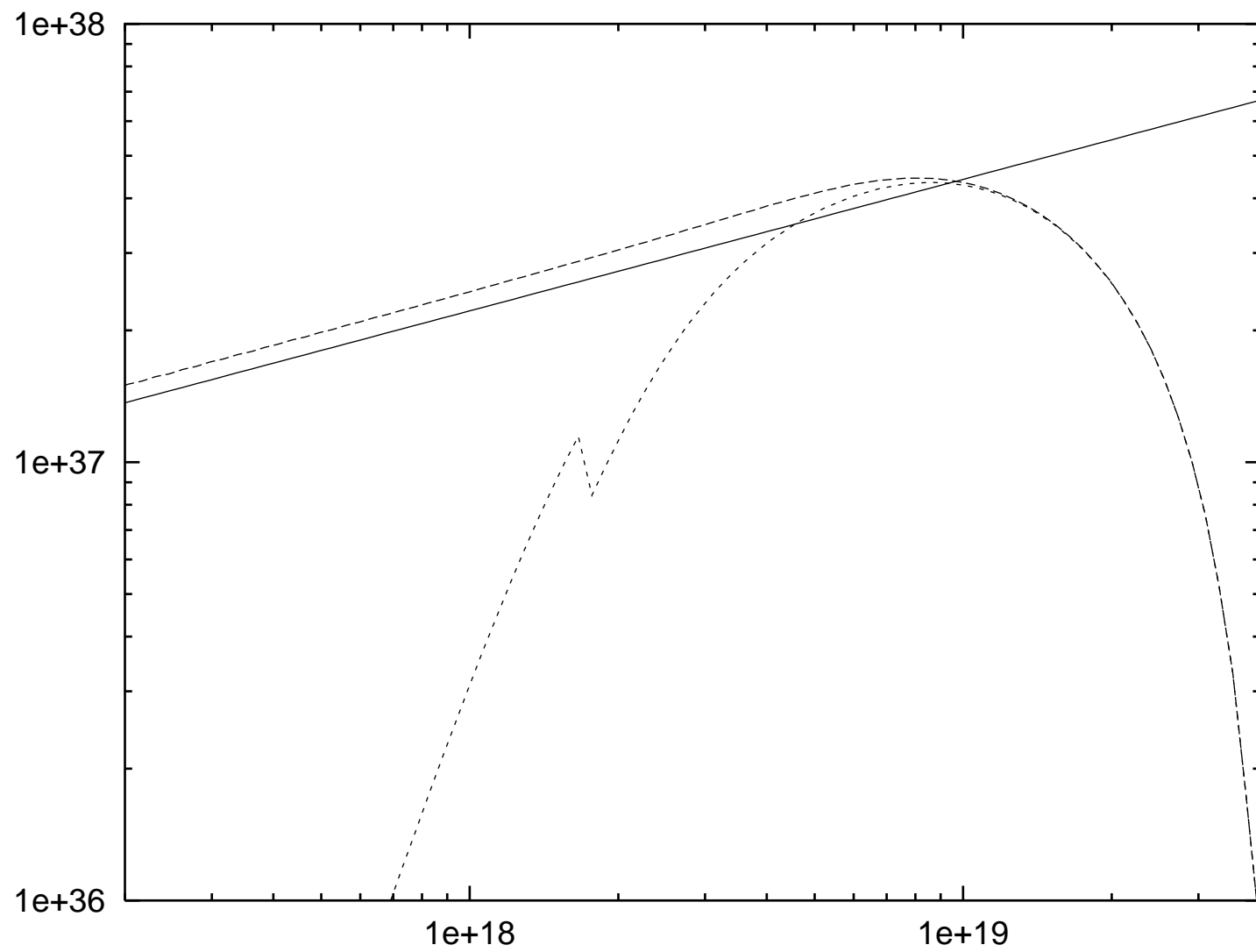












Ratio of Disk to Keplerian Angular Momentum

